Contents lists available at ScienceDirect



Geochimica et Cosmochimica Acta

journal homepage: www.elsevier.com/locate/gca



Molecular dynamics simulation and equation of state of the NaCl-H₂O system from 573 to 1573 K, 1 to 30 kbar, and 0 to 1 m fraction of NaCl

Zhenhao Duan a, Danfei Cheng b, Zhigang Zhang C, I-Ming Chou D, Haoran Sun L

- ^a Department of Experimental Study Under Deep-sea Extreme Conditions, Institute of Deep-sea Science and Engineering, Chinese Academy of Sciences, Sanya, Hainan 572000. China
- b State Key Laboratory of Deep-Sea Science and Intelligent Technology, Institute of Deep-sea Science and Engineering, Chinese Academy of Sciences, Sanya, Hainan 572000 China
- c Key Laboratory of Earth and Planetary Physics, Institute of Geology and Geophysics, Chinese Academy of Sciences, Beijing 100029, China

ARTICLE INFO

Associate Editor: Gleb S. Pokrovski

Negwords:

Molecular dynamics simulation
Equation of state

H₂O activity

NaCl-H₂O system

PVTx properties

ABSTRACT

The NaCl-H₂O geological fluid system is pervasive in and on the Earth, playing a crucial role in fluid-rock interactions, metamorphic and magmatic processes, and ore deposit formation. Over the past fifty years, extensive research has been conducted on this system, resulting in more than 40 sets of experimental data and the development of over ten models. However, the majority of these studies have been limited to pressures below 5 to 6 kbar, thereby restricting geochemical investigations in the lower crust and upper mantle. To address this limitation, we first conducted molecular dynamics (MD) simulations of the pressure-volume-temperaturecomposition (PVTx) properties of NaCl-H2O solutions. Utilizing a non-rigid, flexible RWK2 potential, we explored an extensive P-T range, from approximately 1 to 30 kbar and from 573 K to 1573 K. Based on the simulated PVTx data and supplemented by a limited number of experimental data points, we developed an equation of state (EOS) for the NaCl-H₂O system. This EOS covers a wide range of conditions, extending from 1 kbar to 30 kbar and from 573 K to 1573 K. It also spans the compositional range from pure water to pure NaCl melts. The accuracy of this EOS is comparable to the most reliable existing models for pressures from 1 to 5 kbar, and it closely aligns with experimental data from 5 kbar up to 45 kbar. From the EOS, we have derived several important thermodynamic models that offer potential applications in geochemical and geophysical studies. These include a fugacity model for calculating H₂O activities, which is derived from the EOS of the NaCl-H₂O system and should have broad applications in fluid-rock interactions and mineral solubility studies. Additionally, we developed an electrical conductivity model for investigating crustal and upper mantle fluids. This model is simpler, more precise, and applicable over a wider P-T range compared to existing models. To demonstrate the practical utility of these models, we provide several illustrative examples of their application in geochemical and geophysical contexts, highlighting their versatility and reliability in addressing complex geological phenomena.

A computer program implementing the EOS is available on our new website: https://efs.idsse.ac.cn/module1/binary/h2o-nacl/EOS.html.

1. Introduction

The study of the physicochemical properties of salt or electrolyte aqueous solutions has been one of the most active research areas since the last century (e.g., Adams, 1931; Abdulagatov et al., 1998; Keevil, 1942; Moore and Ross, 1965; Pitzer and Li, 1983; Pitzer et al., 1984; Bodnar, 1985; Pitzer and Pabalan, 1986; Chou, 1987; Yardley and Graham, 2002; Driesner, 2007; Li et al., 2008; Steele-MacInnis et al., 2012; Manning and Aranovich, 2014; Fowler and Sherman, 2020; Li

et al., 2024; Schulze et al., 2024). With various objectives, such as chemical extraction, electric power generation, environmental remediation, theoretical development, and most importantly, geochemical applications, many experimental scientists have conducted tens of thousands of measurements on various aqueous fluid systems that may contain electrolytes (or ions or salts), gases, and dissolved minerals. These data are so valuable that the most prominent research teams have spent years compiling them into packages, such as those produced by Robie and Hemingway (1995), Helgeson and colleagues, Parkhurst and

E-mail address: zduan@idsse.ac.cn (Z. Duan).

^{*} Corresponding author.

Appelo (1999), and those published by IUPAC and NIST. Unlike other research areas, geochemical applications involve large pressure-temperature domains, requiring data covering a wide pressure-temperature-composition range. However, the current experimental data are far from sufficient to quantitatively interpret various processes in fluid-rock interactions, the carbon cycling, seawater acidification, deep-sea chemical reactions and transportation, and pollutant geochemical behavior. Even for systems as simple as pure water, scarce data can be found for pressures above 10 kbar (about 35 km below Earth's surface), not to mention other water–gas-salt systems. The lack of data and models hinders the quantitative advancement of geochemical research towards the deep crust and mantle.

For example, for many years, the widely used geochemical software package SUPCRT92, developed based on a series of seminal articles by Helgeson and colleagues (Helgeson et al., 1978; Johnson et al., 1992; Shock et al., 1992, 1997; Sverjensky et al., 1997), and its derivatives (e. g., SUPCRTBL by Zimmer et al., 2016), were limited to pressures below 5 kbar. It was not until about ten years ago that Sverjensky et al. (2014) extended it to 60 kbar as DEW model based on the equation of state (EOS) of water developed by Zhang and Duan (2005). The parameters of the ZD EOS were evaluated mainly from the results of molecular dynamics (MD) simulations. The DEW model serves as a key example of constructing equations of state (EOSs) from molecular dynamics (MD) simulations, enabling predictions under conditions with limited experimental data.

Over the past forty years, both classical molecular simulation and the first-principle simulation have been demonstrated to be useful tools in predicting thermodynamic and kinetic properties (e.g., Belonoshko and Saxena, 1991a, 1991b; Duan et al., 1995; Zhang and Duan, 2005; Pan et al., 2013; Sakuma and Ichiki, 2016; Mei et al., 2019; Fowler and Sherman, 2020; Pan and Galli, 2020; Schulze and Jahn, 2024). As stated by Fowler and Sherman (2020) that Ab initio molecular dynamics simulations based on density functional theory do not require model interatomic potentials and may reveal chemical reactions associated with bond making and breaking (Lan and An, 2021) and vibrational spectroscopy (Ditler and Luber, 2022). However, they are fundamentally limited by the accuracy of the approximate exchange-correlation potential used to describe interelectronic interactions. On the other hand, the classical simulation may have better predictability for bulk properties as shown in Zhang and Duan (2005) and Fowler and Sherman (2020) in the modest temperature and pressure range. Probably in the near future one cannot be replaced by the other.

Although there are many possible ionic-salt systems in nature, the NaCl-H₂O system is by far the most frequently encountered salt-bearing (electrolyte) aqueous geological fluid, with NaCl concentrations varying from dilute to highly concentrated. Its ubiquitous presence and crucial role in numerous geological processes, including fluid-rock interactions (e.g., Newton and Manning, 2000; Shi et al., 2024), metamorphic processes (e.g., Aranovich and Newton, 1996; Huang and Sverjensky, 2019; Cheng et al., 2019, Qiu et al., 2021), diamond formation (e.g., Sverjensky and Huang, 2015); ore-deposit formation (e.g., Bodnar, 1995; Shu et al., 2021), dehydration-decarbonization in subducting slabs (e.g., Zheng, 2009; Mantegazzi et al., 2013), and especially, the formation of fluid inclusions in minerals used to study the formation temperatures, pressures, and compositions of minerals and rocks (e.g., Bakker, 2003; Ni et al., 2006; Mao et al., 2023), have received significant attention. Consequently, this binary water-electrolyte system has been extensively examined through both experimental and theoretical investigations, with over 40 experimental datasets published since the 1960s.

As comprehensively summarized by Pitzer et al. (1984), Bischoff and Pitzer (1989), Bischoff (1991), Anderko and Pitzer (1993), Driesner and Heinrich (2007), Driesner (2007), Mao and Duan (2008), and Mao et al. (2010, 2015), the majority of these studies are limited to pressures below 5 kbar, with only a few extending to 6 kbar, which corresponds to a depth of approximately 18 km beneath Earth's surface. Table 6 in Mao et al. (2015) listed 38 such *PVTx* datasets, but some important

contributions such as that of Bodnar (1985) were not included. The only volumetric data up to high temperature and pressure are from the acoustic volumetric data of Mantegazzi et al. (2013), which span from 5 kbar to 45 kbar but are limited to below 673 K and the isochores of Li et al. (2024), which extend up to 12 kbar.

Therefore, the ultimate goals of this study are: (1) to demonstrate the predictability of MD simulations in the study of thermodynamic properties of geological fluids using the non-rigid RWK2 potential over a large PTx range; (2) to develop an accurate EOS of the NaCl-H₂O system which covers a much larger PTx range than previous models; (3) to address some important geochemical and geophysical applications of the EOS.

2. Molecular dynamics simulation of the NaCl-H $_2$ O system with RWK2

Key to MD simulations is intermolecular or interatomic forces, which are derived from potential functions. Hence, water molecular potential is essential in the simulation of aqueous fluids (e.g., Duan et al., 1995; Zhang and Duan, 2005; Mei et al., 2019). Over the last half-century, various potential functions for water molecules have been developed for studies in chemistry, material science, and biology to gain insights into physical and chemical processes, as well as to facilitate predictions of thermodynamic properties. The final MD simulation results depend on two factors: the choice of molecular potential and the simulation setup.

2.1. The choice of H_2O molecular potential: The non-rigid RWK2 potential

For the NaCl-H₂O system, there are interactions between H₂O-H₂O, Na⁺-Na⁺, Cl⁻-Cl⁻, Cl⁻-Na⁺, Na⁺-H₂O, and Cl⁻-H₂O. The Na⁺ and Cl⁻ ions are considered as point charges with mass, and H₂O has both intra-and inter-molecular interactions. The total potential energy (U_{tot}) would be:

$$U_{tot} = U_{H_2O - H_2O} + U_{H_2O - Na^+} + U_{H_2O - Cl^-} + U_{Na^+ - Na^+} + U_{Cl^- - Cl^-} + U_{Na^+ - Cl^-}$$
(1)

The first term on the right is the H₂O-H₂O potential, which is the most important and most difficult to depict. As reviewed by several research groups (e.g., Duan et al., 1995; Sherman and Collings, 2002; Zhang and Duan, 2005; Vega and Abascal, 2011), more than 40 water potentials have been proposed over the past four decades. Vega and Abascal (2011) gives TIP4P a higher mark than SPC/E, but in the high P-T supercritical range, SPC/E yields a better accuracy in prediction of the PVTx properties as shown in Figs. 2 and 6 of Zhang and Duan (2005). Using the simulated data with SPC/E, Zhang and Duan (2005) got an EOS for pure water almost as accurate as the NIST EOS (Wagner and Pruß, 2002) for water at pressures above 2 kbar. The rigid SPC/E model has been used in numerous studies (e.g., Smith and Dang, 1994; Zhang and Duan, 2005; Mei et al., 2019; Fowler and Sherman, 2020). However, we choose the RWK2 in the simulations of the H2O-NaCl mixtures for the following reasons: (1) as studied by Fowler and Sherman (2020), the SPC/E potential exhibits higher deviations from experimental data (ranging from 4 % to 5 % in density) as the temperature increases to 400 °C and the pressure rises to 1 GPa; (2) The RWK2 model more closely represents the true behavior of water molecules, allowing for flexible intramolecular bond and angle motions in H2O; (3) The positioning of the negative charge in the RWK2 model partially accounts for polarization effects in water molecules. (4) The flexibility of intramolecular motions in the RWK2 model enables us to study the spectra of water molecules as functions of PTx and the liquid structures of salt aqueous solutions for further research. (5) Our study aims to cover a much wider PTx range, as previously stated. The switch from SPC/E to RWK2 for the binary has indeed resulted in better PVTx predictions in the high T-P

range, as compared with the the model of Mao et al. (2015), which improved the accurate model of Driesner (2007) by replacing the model of Haar et al. (1984) with the most updated NIST water EOS (Wagner and Pruß, 2002). The MD simulated data construct the basis for developing an eventual equation of state (EOS).

Although the RWK2 potential was obtained by least square fitting to the static lattice energies and bulk moduli of ices and the second virial coefficient of steam (Reimers et al., 1982; Coker and Watts, 1987), it was proven to be capable of predicting high *PVT* properties (Duan et al., 1995, 2004). For the reasons above, we choose the RWK2 potential in this study. In this interaction potential, two hydrogen nuclei are located at RH1 and RH2, each carrying a positive charge q (0.6), while a negative charge, -2q (-1.2), is situated at a bisection point in the plane of H-O–H of water molecules: $R_{-O} = R_O + \delta(R_{H1} + R_{H2} - R_O)$, where δ is a constant with a value of 0.22188758 in atomic unit. The location of the negative charge R_{-O} is subject to change in accordance with the geometry of the water molecule, which, in turn, modifies with the molecular environment. This change, to some extent, weakens the polarization of water molecules.

The ionic potentials are based on Smith and Dang (1994). The RWK2 potential is more concisely summarized in equations (2)-(7) with parameters (in atomic units) listed in Table 1.

$$U_{H_2O-H_2O} = U_{intra} + U_{inter} \tag{2}$$

$$U_{\text{intra}} = \sum_{i=1}^{3} D_i (1 - e^{-\alpha s_i})^2 + f_{12} s_1 s_2$$
(3)

$$s_i = r_{\text{OH}_i} \cos\left(\frac{\theta - \theta_0}{2}\right) - R_0, \quad i = 1, 2$$
(4a)

$$s_3 = \frac{r_{\text{OH}_1} + r_{\text{OH}_2}}{R_0} \sin\left(\frac{\theta - \theta_-}{2}\right) \tag{4b}$$

$$U_{\text{inter}} = \sum_{i,j}^{3} \frac{q_i q_j}{r_{ij}} + \sum_{OO} A_{OO} e^{-\alpha_{OO} r_{OO}} + \sum_{H,H} A_{HH} e^{-\alpha_{HH} r_{HH}} +$$

$$\sum_{\text{O.H}}\!\!A_{\text{OH}}e^{-\alpha_{\text{OH}}(r_{\text{OH}}-r_0)}\big[e^{-\alpha_{\text{OH}}(r_{\text{OH}}-r_0)}-2\,\big]+$$

Table 1The parameters of RWK2 potential.

Parameters	Value(atomic unit)
R_0	1.8088
θ_0	104.52
$D_{1,2}$	0.20916
D_3	0.15660
$\alpha_{1,2}$	1.13315
α_3	0.70600
f_{12}	-0.00676
$A_{ m HH}$	1.00703
$\alpha_{ m HH}$	1.73603
q_H	0.6000
q_O	-1.2
A_{OH}	0.0033045
$lpha_{ m OH}$	3.89559
R_m	3.09500
C_6^*	62.45134
C_8	1344.45317
C_{10}	50014.91123
A_{OO}	5107.32897
$a_{ m OO}$	2.63108
а	1.99152
b	0.098016
β	2.326
c	0.94834
δ	0.22188758
β	0.88397

$$\sum_{0.0} \left\{ -f \left[C_6 \left(\frac{g_6}{r_{00}} \right)^6 + C_8 \left(\frac{g_8}{r_{00}} \right)^8 + C_{10} \left(\frac{g_{10}}{r_{00}} \right)^{10} \right] \right\}$$
 (5)

$$f = 1 - (cr_{00})^{\beta} e^{-cr_{00}} \tag{6}$$

$$g_n = 1 - e^{-\left(ar_{00}/n + br_{00}^2\right)/\sqrt{n}} \tag{7}$$

The other five terms on the right of Eq. (1) are all pair additive potentials of the sum of Lenard-Jones plus Coulombic interactions:

$$U_{ij} == \sum_{i} \sum_{j} \left\{ 4\varepsilon_{ij} \left[\left(\frac{\sigma_{ij}}{r_{ij}} \right)^{12} - \left(\frac{\sigma_{ij}}{r_{ij}} \right)^{6} \right] + \frac{q_{i}q_{j}}{r_{ij}} \right\}$$
(8)

The parameters of Eq. (8) are listed at the end of Table 2. Notice that the the acting site of the H_2O molecule is the nuclei on the oxygen, and that the Smith and Dang ion-water interaction parameters are slightly modified. All mixing parameters are calculated by the Lorentz-Berthelot combining rule:

$$\varepsilon_{ij} = \sqrt{\varepsilon_i \varepsilon_j} \tag{9}$$

$$\sigma_{ij} = \frac{\sigma_i + \sigma_j}{2.0} \tag{10}$$

2.2. Initial simulation setup and procedures: programming and execution

A typical MD simulation generally involves the following steps: (1) the initial setup, wherein a specified number of molecules are placed into a designated simulation box; (2) the execution of a dynamic program that simulates the time-evolution of molecular movements within the box, once the program parameters are properly configured; (3) the observation and recording of specific variables during the simulation run; and (4) the analysis of the final results.

In this study, we programmed a constant molecular number-volumeenergy (NVE) algorithm, allowing easy isochoric simulation and reliability checks. The simulation program employs conventional periodic boundary conditions (PBC) and the minimum image convention in a cubic box for the calculation of inter- and intramolecular distances. Long-range electric energy and forces are calculated with the Ewald summation. The Verlet algorithm (Allen and Tildesley, 1987) is used to integrate the Newton equations of motion of atoms and calculate velocities. Special care was taken in programming the intramolecular motions for the non-rigid flexible RWK2 potential. Since the negative charge is located at a bisection point of the H₂O molecule, its position depends on the coordinates of the two hydrogen atoms and the oxygen atom. This means that the negative charge could be located outside the simulation box while the H or O could be located inside the box. Therefore, extra attention must be paid to programming the positions of these atoms under periodic boundary conditions. Additionally, when scaling the simulation box size, care should be taken to ensure that all H₂O molecules remain intact. The program allows changing temperature by scaling velocities and changing pressure by scaling box size.

In this study, we introduce 1664 $\ensuremath{\text{H}_2\text{O}}$ molecules along with a specific

Table 2
L-J parameters and charges for Eq. (8).

Parameters	Value (atomic unit)
$\varepsilon_{ m H_2O}$	2.430×10^{-4}
$\sigma_{ m H_2O}$	5.9905
ε_{Na^+}	2.038×10^{-4}
σ_{Na^+}	5.0473
$arepsilon_{ ext{Cl}^-}$	1.568×10^{-4}
σ_{Cl^-}	7.750
q_{Na^+}	1
q_{Cl^+}	-1
q_H	0.6
q_{-O}	-1.2

number of Na $^+$ and Cl $^-$ ions, corresponding to 10 wt%, 20 wt%, and 33 wt% NaCl concentrations in the aqueous solution, into a cubic simulation box for constant NVE simulation (constant number of particles, volume and the total energy, which equals potential energy + kinetic energy).

The time step for all simulations is then set at 0.75 fs. For the first run, the total pre-equilibrium process takes about 40 ps for the first run, 10 ps of pre-equilibrium for the rest of runs, followed by 25 ps of simulation for data collection, during which the instantaneous temperature and pressure are calculated and averaged.

$$T = \frac{2E}{3Nk_B} andP = \frac{Nk_BT}{V} - \frac{1}{3V} \sum_{i} \sum_{j>i} r_{ij} \frac{\partial U_{ij}}{\partial r_{ij}}$$

$$\tag{11}$$

where E is the total kinetic energy, k_B is the Boltzmann constant, U_{ij} is the potential energy between particles i and j, and r_{ij} is the distance between particles i and j. The final configuration of the first run was used as the start of the next run.

2.3. Simulated PVTx properties for the NaCl- H_2O system over a large P-T range

After developing the MD computer simulation program with the relatively complex RWK2 potential, the ionic potentials, and the initial input setup, we carried out 282 NVE simulations and obtained the same number of *PVTx* data as shown in Table 3. As shown in Fig. 1, the simulated results are very close to experimental data up to 1273 K and 12kbar. Fig. 2 shows that the simulated points generally follow slightly concaved lines, implying that the independent simulations show consistent results with small calculation uncertainties. Fig. 3 shows that the EOS, evaluated from the MD data with a small number of experimental data, is highly consistent with experimental data up to 45 kbar.

However, in most cases, there is no experimental data for comparison, or in cases where data do exist, the data themselves are subject to significant uncertainties, which we may not necessarily be aware of. Statistical theory suggests that a model based on multiple datasets will smooth out the measurement noise, and if the same measurements are repeated N times, the error will be reduced to:

$$\frac{err_s}{\sqrt{N}}$$
 (12)

Where err_s represents the error of a single measurement, and N denotes the number of repeated measurements. This is one of the reasons why a robust model may be more reliable than a randomly selected experimental dataset. For instance, the NIST model of water (Wagner and Pruß, 2002) achieves an accuracy of approximately 0.1 % in molar volume, which is more precise than any individual dataset because it is based on multiple datasets. It is noteworthy that the EOS of Zhang and Duan (2005) attains an accuracy comparable to the NIST H₂O model above 1 kbar without fitting any data below 10 kbar. The ability to extrapolate is one of the strengths of a predictive model with a theoretical foundation. Such a model can extrapolate and mitigate some experimental noise.

From the perspective of MD, it would be imprudent to seek results more accurate than a single experimental dataset over a very large *PTx* range for three reasons: (1) three-body interactions in a molecular system cannot be fully captured by pair-additive potentials such as RWK2 or SPCE; (2) the charge on a molecule or ionic particle can be polarized, which cannot be accounted for by pair-additive potentials, although RWK2 mitigates polarization effects by positioning its negative charge according to the distribution of surrounding charges. Generally, most experimental *PVTx* measurements have about 1–2 % uncertainty in molar volumes.

For the reasons discussed above, we do not conduct point-by-point comparisons between simulated data and individual datasets, except for the recent data from Li et al. (2024), which were not included in previous models, as illustrated in Fig. 1. As shown in Fig. 1, the recent isochoric measurements are well-predicted by our MD simulations. In the *PTx* range covered by the data, our MD simulation results are consistent with the experimental data from Li et al. (2024).

In order to assess the reliability of the simulated results in Table 3, we choose the EOS of Zhang and Duan (2005) as the standard for pure water to compare with and select the model of Mao et al. (2015) as the standard for the NaCl-H₂O mixture system to compare with. The EOS of water proposed by Zhang and Duan (2005) has been demonstrated to be highly consistent with the model of Wagner and Pruß (2002) below 20 kbar (Table 4), which was selected by NIST and IAPWS as the standard water model. Furthermore, the ZD EOS aligns with the experimental data above 10 kbar, thereby serving as the basis for the DEW model developed by Sverjensky et al. (2014), extending the HKF model from 5 kbar to 60 kbar, and as a standard by Pan et al. (2013) to assess the accuracy of the DFT-PBE functional they used to calculate the dielectric constant of water under mantle *P-T* conditions. For the NaCl-H₂O system, we employ the model of Mao et al. (2015) for comparison.

The model by Mao et al. (2015) was an improvement over the model by Driesner (2007), which has been considered the most accurate H_2O -NaCl model below 5kbar. Through the adoption of the IAPWS-95 pure water equation of state (EOS) developed by Wagner and Pruß (2002) and substitute it for the model of Haar et al (1984), the model of Mao et al. has also been validated against nearly all available experimental data of nearly forty datasets with thousands of data points, demonstrating uncertainties of less than 1 % in density below 1 kbar and an average of 2 % in density above 1 kbar, as demonstrated by their Fig. 1.

Most simulated results, excluding simulations at very high densities (molar volumes smaller than $16~{\rm cm^3/mole}$) and very low densities (molar volumes higher than $28~{\rm cm^3/mole}$), are well predicted in the pressure range from about 1 kbar to 30 kbar, with average deviations of about 1.5 %, which is comparable to the uncertainty in experimental observations as discussed above. It is worth noting that H_2O may become more ionized at high pressures, but extrapolation from the limited data (Hamann, 1963; Arcis et al., 2024) suggests that the ionization fraction of water will not be higher than 1 % below 30 kbar, which will not appreciably affect the *PVT* properties of the NaCl- H_2O mixtures.

Simulation errors increase as pressure decreases, a phenomenon known as the "tail effect" of empirical potentials. This occurs because, at low densities, the average molecular separation becomes large enough to enter a weak attractive region where classical potentials are notoriously inaccurate. As noted by Kaplan (2006), at these distances ($R \gtrsim \lambda$), the dispersion interaction is significantly influenced by vacuum electromagnetic field fluctuations. A complete model must account not only for the fluctuating dipoles of the interacting molecules but also for the dipole moments induced in them by the vacuum field, a quantum mechanical effect that classical potentials fail to capture. Consequently, widely used models like SPC/E and TIP4P all exhibit this tail effect, which can sometimes manifest as unphysical negative pressures at low temperatures, signaling a spurious phase transition. Fig. 2 shows that the independent simulated points on the same isochore always align along the same line well, indicating the reliability of the simulations. Notably, isochoric lines are not necessarily straight but are slightly concave. The curvature is relatively small, and the lines can be approximated as straight within a span of about 10 kilobars; however, caution should be warranted when the pressure span exceeds 10 kbar.

3. Equation of state of the H₂O-NaCl system from 573 to 1573 K, 1 to 30 kbar, and 0 to 1 $x_{\rm NaCl}$

An equation of state (EOS) is a mathematical function that describes the relationship between pressure, volume, temperature, and composition of substances. Theoretically, many physicochemical properties can be derived from an EOS, such as phase properties (immiscibility,

Table 3 The MD simulated PVT properties of the H_2O -NaCl system.

T (K)	P (bar)	$V (cm^3/mc^3)$		dev%	T (K)	P (bar)	$V (cm^3/me)$		dev%
Pure water 471.7	22,952	D24 14	ZD05 13.78	1.57	811	6662	D24 20	ZD05 19.97	0.15
635.6 800.8	32,266	14	13.52	3.43	812.2	6588 9284	20 20	19.99 19.58	0.05
1076.2	40,759 53,635	14 14	13.38 13.27	4.43 5.21	924.1 926.7	9360	20	19.57	2.1 2.15
1424.9	68,227	14	13.23	5.5	1066.4	11,514	20	19.7	1.5
1573	73,622	14	13.22	5.57	1282.1	15,280	20	19.62	1.9
467.9	13,577	15	14.96	0.27	1287.6	15,538	20	19.55	2.25
638.4	21,606	15	14.61	2.6	1346.8	16,237	20	19.65	1.75
834.1	29,896	15	14.42	3.87	1572.4	19,688	20	19.67	1.65
1091.6	37,698	15	14.51	3.27	705.3	2365	23	22.91	0.39
1531.6	50,350	15	14.62	2.53	705.3	2227	23	23.41	-1.78
483.8	8668	16	15.57	2.69	705.6	2196	23	23.27	-1.17
628	13,542	16	15.87	0.81	848.9	4273	23	22.82	0.78
628.2	13,349	16	15.91	0.56	849	4051	23	23.28	-1.22
790.2 898.7	19,902 23,130	16 16	16.05 15.54	-0.31 2.88	854.3 897.2	4619 4804	23 23	22.55 23.07	1.96 -0.3
899.3	23,001	16	15.57	2.69	911.5	4857	23	23.16	-0.3 -0.7
1245.5	34,219	16	15.57	2.69	959.4	5615	23	23.06	-0.26
1252.4	34,876	16	15.56	2.75	959.4	5615	23	23.06	-0.26
538.5	6886	17	17	-0.06	959.4	5615	23	23.06	-0.26
642.1	9936	17	16.86	0.82	968.4	5743	23	22.79	0.91
749.4	13,308	17	16.68	1.88	970.9	5941	23	22.77	1
922.3	17,952	17	16.62	2.24	1077	6970	23	23.21	-0.91
1129.5	23,061	17	16.6	2.35	1079	6971	23	23.21	-0.91
1570	33,523	17	16.55	2.65	1145.4	8363	23	22.61	1.7
397.5	195	18	18.3	-1.67	1145.4	8363	23	22.61	1.7
441.8	1652	18	18.45	-2.5	1146.7	8339	23	22.65	1.52
492.4	2892	18	18.31	-1.72	1146.7	8339	23	22.65	1.52
495.1	2866	18 18	18.38 18.32	-2.11 -1.78	1158.4	8397 8397	23	22.7	1.3 1.3
542.8 564.4	3905 4525	18	18.25	-1.78 -1.39	1158.4 1158.4	8397 8397	23 23	22.7 22.7	1.3
595.7	5404	18	18.11	-0.61	1368.9	11,162	23	22.57	1.87
613.9	5697	18	18.2	-0.01 -1.11	1368.9	11,162	23	22.57	1.87
633.9	6444	18	18.09	-0.5	1372.1	11,254	23	22.52	2.09
635.5	6922	18	17.89	0.61	1372.1	11,254	23	22.52	2.09
655.6	7473	18	17.85	0.83	1387.3	11,205	23	22.71	1.26
655.6	7473	18	17.85	0.83	1387.3	11,205	23	22.71	1.26
662.7	7507	18	17.91	0.5	1449	12,149	23	22.54	2
745.2	9395	18	17.88	0.67	1449	12,149	23	22.54	2
745.6	9711	18	17.77	1.28	774.6	1972	26	26.21	-0.81
767.8	9717	18	17.95	0.28	774.6	1972	26	26.21	-0.81
906.4	13,493	18	17.51	2.72	985	4193	26	25.94	0.23
914	14,341	18	17.58	2.33	985	4193	26	25.94	0.23
996.4 1030.2	15,549 16,317	18 18	17.67 17.65	1.83 1.94	1304.7 1304.7	7439 7439	26 26	25.7 25.7	1.15 1.15
1292.4	22,710	18	17.6	2.22	686	348	28	28.48	-1.71
1292.4	22,210	18	17.58	2.33	686	348	28	28.48	-1.71
1320.3	22,701	18	17.57	2.39	781	1554	28	27.71	1.04
1570	27,160	18	17.65	1.94	781	1554	28	27.71	1.04
591.3	2381	20	20.31	-1.55	972.5	3400	28	27.45	1.96
598.4	2629	20	20.18	-0.9	972.5	3400	28	27.45	1.96
601.3	2581	20	20.29	-1.45	1266	6056	28	27.44	2
639	3412	20	20.13	-0.65	1266	6056	28	27.44	2
743.2	5653	20	19.81	0.95	1594.1	8713	28	27.49	1.82
753.3	5897	20	19.79	1.05	1594.1	8713	28	27.49	1.82
769.4	6209	20	19.77	1.15	613.9	5697			
10 wt% NaCl		D24	M15		4040.6		D24	M15	
516.5	31,249	14			1312.6	25,192	18		
701	41,652	14			1398	26,940	18		
824.1 1037.2	48,128 58,478	14 14			1578 476.7	31,180 -89	18 20		
1563	79,382	14			476.7	-89 -89	20		
507.9	19,039	15			527.9	-89 950	20	20.45	-2.25
637.9	25,059	15			633.8	3330	20	20.01	-2.25 -0.05
817.9	33,310	15			637.4	3090	20	20.25	-1.25
1114.2	45,210	15			791.7	6507	20	19.87	0.65
1555	60,095	15			792.6	6396	20	19.89	0.55
450	9695	16			861.2	8456	20	19.74	1.3
587.2	14,722	16			979.4	10,517	20	19.95	0.25
608.6	16,856	16			1244	15,544	20	19.96	0.2
608.7	15,641	16			1244	15,544	20	19.96	0.2
784.4	22,381	16			1291 1570	17,005 21,946	20		
822.4	23,302	16					20		

(continued on next page)

Table 3 (continued)

T (K)	P (bar)	V (cm ³ /mo	le)	dev%	T (K)	P (bar)	V (cm ³ /mc	ole)	dev%
Pure water		D24	ZD05				D24	ZD05	
471.7	22,952	14	13.78	1.57	811	6662	20	19.97	0.15
825.6	24,956	16			535.7	-429	23		
1124.3	33,801	16			587.9	304.7	23	23.34	-1.48
1134.1	36,012	16			641.1	1145.5	23	22.79	0.91
1454.8	44,685	16			651.6	1029	23	23.39	-1.7
446.7	2562	18	18.12	-0.67	653.3	981	23	23.57	-2.48
450	2041	18	17.78	1.22	698.6	1567	23	23.49	-2.13
458.2	2460	18	18.25	-1.39	699.9	1561	23	23.49	-2.13
459.9	2083	18	18.45	-2.5	714.6	2315.4	23	22.52	2.09
554.6	5686	18	17.77	1.28	775	2790	23	23.05	-0.22
678.8	8163	18	18.21	-1.17	783.5	2963	23	22.96	0.17
680.3	7995	18	18.28	-1.56	855.1	3892	23	23.03	-0.13
680.6	8045	18	18.26	-1.44	856.7	4104	23	22.8	0.87
680.6	8062	18	18.26	-1.44	1006.9	6091	23	22.93	0.3
680.6	8062	18	18.26	-1.44	1131.9	7715	23	23.01	-0.04
719.4	9658	18	10.20	-1.44	1140.7	8556	23	22.41	2.57
836.7			10.16	-0.89			23 23	22.41	2.57
	13,076	18	18.16		1360.8	11,072		*	
836.7	13,076	18	18.16	-0.89	1446.7	12,324	23		1.50
838.8	13,124	18	18.17	-0.94	1446.7	12,324	23	22.65	1.52
840	13,592	18	18.07	-0.39	1463.4	12,413	23	~	
840	13,592	18	18.07	-0.39	1465.5	12,543	23		
968.2	16,666	18			835.7	1506	28	27.52	1.71
1266.2	24,355	18			1049.4	3682	28	27.53	1.68
1306.6	24,469	18			1384.3	6456	28	27.49	1.82
1307.5	24,525	18			1398	26,940			
20 wt% NaCl		D24	M15				D24	M15	
358.7	7594	16			889.6	9502	20	20.07	-0.35
499.8	13,700	16			954.2	11,066	20	20.09	-0.45
569.8	16,779	16			971.8	11,348	20		
571.3	16,642	16			1091	13,595	20	20.31	-1.55
717.5	22,486	16			1092	13,600	20	20.31	-1.55
742.9	23,924	16			1119.4	13,913	20		
743.7	24,013	16			1346.8	18,721	20		
1002.7	33,050	16			1362	18,462	20		
1004.2	33,470	16			1570	22,249	20		
1074	36,200	16			530.8	72	21	21.5	-2.38
370.4	-60	18			535.2	223	22	21.72	1.27
446.8	3119	18	18.1	-0.56	648.1	1356	22	22.19	-0.86
672.3	9656	18			795.3	3844	22	21.98	0.09
970.1	17,400	18			613	323	23	23.42	-1.83
1247	25,547	18			613.7	314	23	23.42	-1.83
1569	33,900	18			676.7	1210	23	23.12	-0.52
471	-552	20			732.2	1982	23	23.03	-0.13
540	1239	20	20.32	-1.6	829.2	3405	23	22.95	0.22
542.1	1164	20	20.42	-2.1	834.5	3541	23	22.89	0.48
578	1507	20	20.7	-2.1 -3.5	842.6	3769	23	22.78	0.46
584	2356	20	20.09	-0.45	940	5519	23	22.45	2.39
678.8	3829	20	20.4	-0.43 -2	1077.8	7265	23	22.98	0.09
679.7	3808	20	20.42	-2 -2.1	1107.8	7565	23	23.3	-1.3
			19.94	-2.1 0.3	1361		23 23	23.3	-1.3
776.7	7008	20				11,072		22.2	0.07
797.2	7214	20	20.05	-0.25	1364.4	11,089	23	23.2	-0.87
807.9	7299	20	20.2	-1	1369.1	11,290	23	23.07	-0.3
811.9	7582	20	20.14	-0.7	1573	14,076	23		

Note: D24 indicates this study, and ZD05 represents Zhang and Duan (2005). For blanks, there is no data or model to compare with.

solubility, and phase equilibrium), volumetric properties (volume, density, and compressibility), thermal properties (enthalpy, heat capacity), and chemical properties (chemical potential, activity, and fugacity). Our experience in the development of models (e.g., Duan et al., 1992a, b, 1995, 1996, 2003; Zhang and Duan, 2005) has demonstrated the efficacy of a well-constructed EOS in interpolating existing data and extrapolating far beyond the *PTx* range of existing data. Therefore, in this study, instead of using empirical models, we employ EOS (semi-empirical) formulation to describe the *PVTx* properties of the NaCl-H₂O system over a much larger *PTx* range than previous models, making the MD-simulated data more accessible to geochemists and filling the gap above 5 kbar up to at least 30 kbar (maybe as high as 50 kbar).

To the best of our knowledge, the only EOS for the NaCl- $\rm H_2O$ system is the EOS proposed by Anderko and Pitzer (1993). This EOS covers the range from 273 K, 1 bar to 1273 K, 5 kbar and is capable of calculating

both *PVTx* properties and liquid–vapor phase equilibria. However, it cannot be extrapolated to higher pressures, and it is a challenge to program their EOS for its complexity. The other models are empirical. The EOS of Duan et al. (1992a, b) has been proven effective for gases and aqueous fluids, yet it has never been used in salt aqueous systems. The formula has been rewritten by Zhang and Duan (2005) as follows:

$$Z = 1 + \frac{B}{V_r} + \frac{C}{V_r^2} + \frac{D}{V_r^4} + \frac{E}{V_r^5} + \left(\frac{F}{V_r^2} + \frac{G}{V_r^4}\right) \exp\left(-\frac{\gamma}{V_r^2}\right)$$
 (13)

$$B = a_1 + \frac{a_2}{T_r^2} + \frac{a_3}{T_r^3} (14a) \qquad C = a_4 + \frac{a_5}{T_r^2} + \frac{a_6}{T_r^3} \quad (14b)$$

$$D = a_7 + \frac{a_8}{T_r^2} + \frac{a_9}{T_r^3} (14c) \qquad E = a_{10} + \frac{a_{11}}{T_r^2} + \frac{a_{12}}{T_r^3}$$
 (14d)

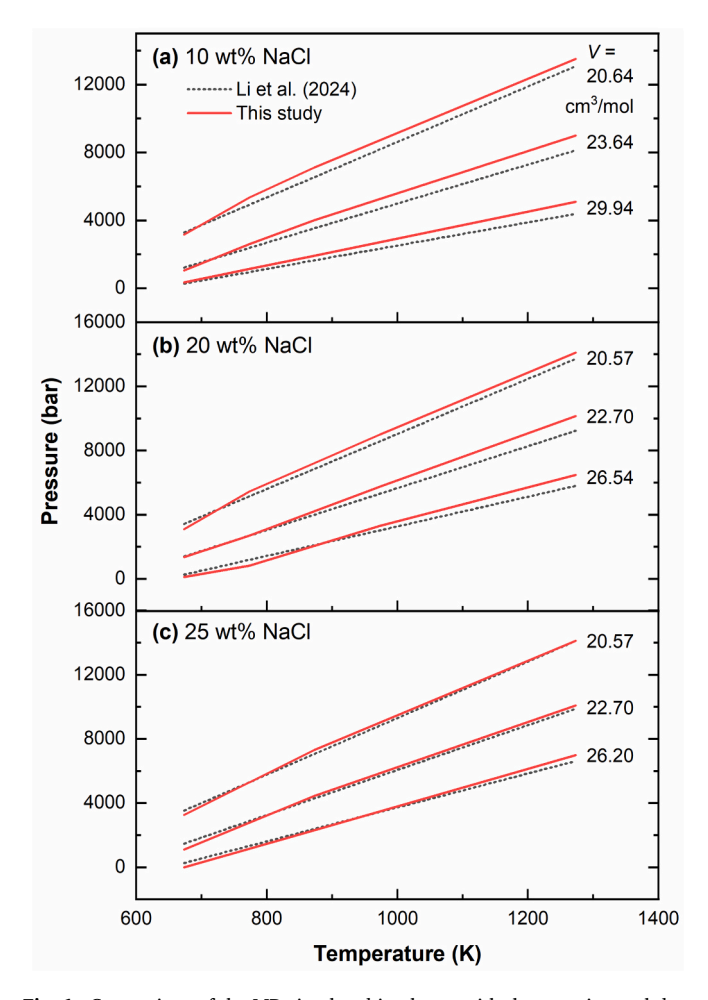


Fig. 1. Comparison of the MD simulated isochores with the experimental data of Li et al. (2024).

$$F = \frac{a_{13}}{T_r} (14e)$$
 $G = a_{14}T_r$ (14f)

$$T_r = \frac{T}{T_c} \qquad V_r = \frac{V}{V_c} \tag{14g}$$

Z is compressibility factor. The coefficients a_1 to a_{14} and γ are parameters to be determined from PVT data for the end members (NaCl and H_2O). Once the end member EOS parameters are determined, a mixing rule can be established for the completion of the EOS for the NaCl- H_2O system.

3.1. EOS of NaCl melt

Utilizing the formula of Tödheide (1980), which was derived from the summarized data of Janz (1980), we obtained liquid NaCl density data up to approximately 1573 K and 7 kbar, similar to Driesner (2007). And then for pressures exceeding 7 kbar, we employed the molten liquid compressibility data from Bockris and Richards (1957) to calculate NaCl liquid density up to about 50 kbar.

$$\rho_{\textit{NaCl,liq}} = \frac{\rho_{\textit{NaCl,liq}}^0}{1 - 0.1 ln(1 + 10 \kappa_{\textit{NaCl,liq}} P)} \tag{15a}$$

$$\rho_{NaCl,liq}^{0} = \frac{58443}{23.772 + 0.018639T \pm 1.9687 * 10^{-6}T^{2}}$$
 (15b)

$$\kappa_{NaCl,liq} = -1.5259*10^{-5} + 5.5058*10^{-8}T$$
(15c)

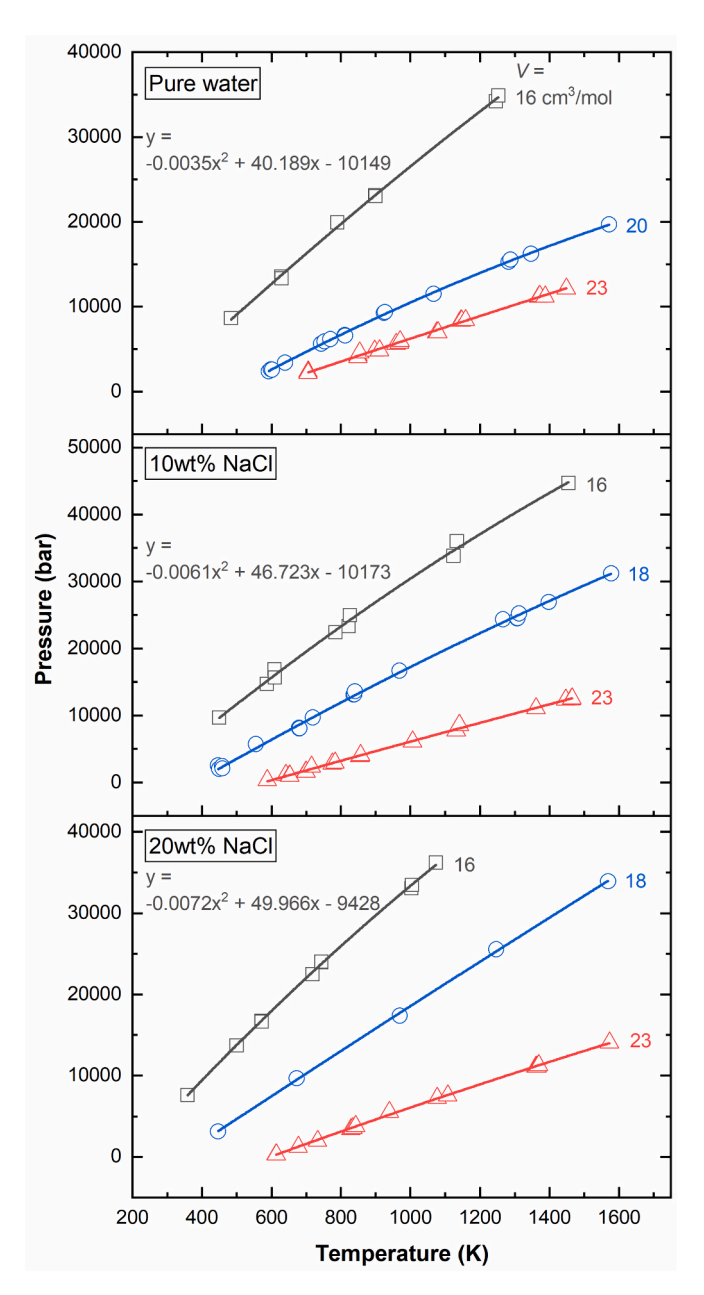


Fig. 2. The isochores drawn from the MD simulated results (the symbols are simulated data from Table 3, and the smoothed curves represent isochores).

 $\rho_{NaCl,liq}$ is halite liquid density at a given temperature and pressure; $\rho_{NaCl,liq}^0$ is halite liquid density at reference pressure (1 bar) in units of kg/m³; $\kappa_{NaCl,liq}$ Liquid NaCl compressibility in unit of bar $^{-1}$. To evaluate the parameters of Eq. (13)-(14), the critical parameters of molten NaCl must be determined from the data of Bockris and Richards (1957) and Kirshenbaum et al. (1962) to best fit the molten NaCl density. The critical parameters are listed in Table 5. With the density data and critical properties available, we can evaluate the parameters of Eq. (14), and the EOS of molten or liquid NaCl is obtained with the parameters listed in Table 5. To test the predictability of the EOS, we compare it with the experimental density data of Van Artsdalen and Yaffe (1955) and the data of Kirshenbaum et al. (1962), showing deviations of less than 0.7 % up to 1500 K, as displayed in Table 6. This demonstrates that the EOS can be used to quantify the *PVT* properties of melts very accurately.

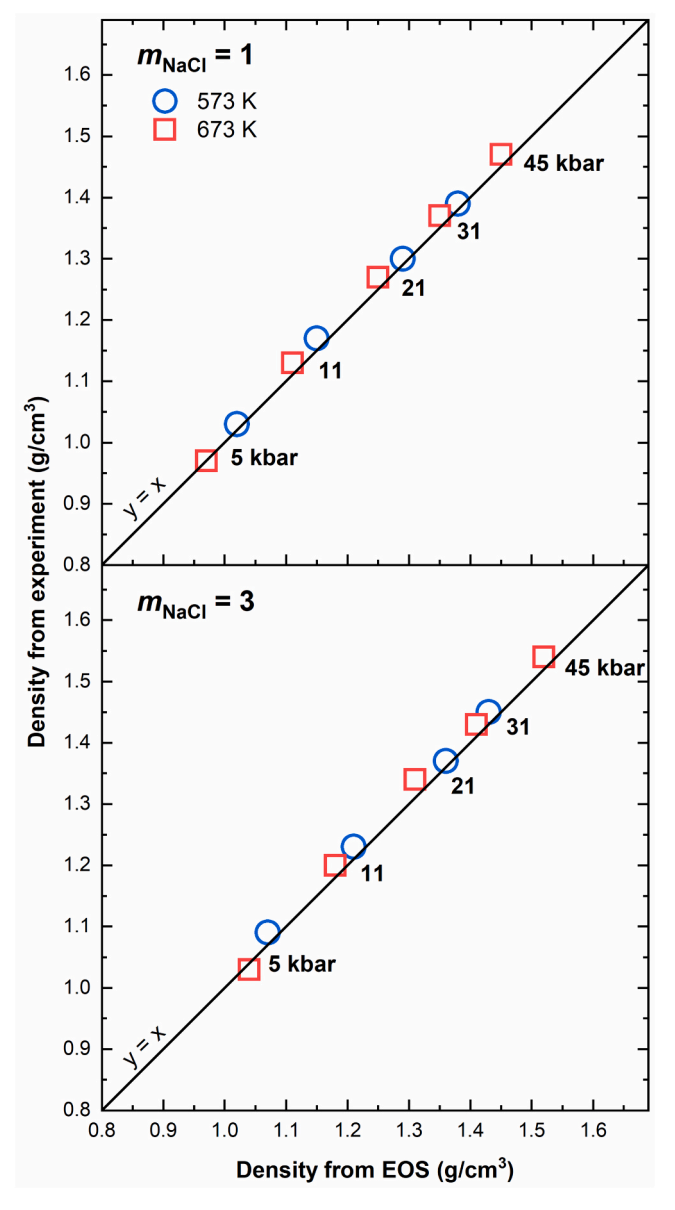


Fig. 3. Comparison of the EOS of this study with acoustic volumetric data (Mantegazzi et al., 2013) at P-T conditions ranging from 5 to 45 kbar and below 673 K with NaCl molality $m_{NaCl}=1,3$.

Table 4 Comparison of the Zhang and Duan (2005) EOS with the NIST EOS (Wagner and Pruß, 2002).

T(K)	P(kbar)	V(cc/mole) NIST (Wagner and Pruß, 2002)	V(cc/mole) Zhang and Duan (2005)
573	1	21.881	21.899
	5	18.102	18.136
	10	16.315	16.338
	20		14.536
773	1	34.085	33.951
	5	20.698	20.786
	10	17.837	17.889
	20		15.458
1073	1	78.088	78.675
	5	25.898	26.067
	10	20.410	20.604
	20		16.962

Table 5 EOS Parameters for H_2O and NaCl (Eq. 14).

Parameters	H_2O	NaCl
a1	$3.49824207 \times 10^{-1}$	-2.6756707
a2	-2.91046273	$4.641389970 \times 10^{-1}$
a3	2.00914688	$-2.516273800 imes 10^{-1}$
a4	$1.12819964 \times 10^{-1}$	$2.449597154 \times 10^{-1}$
a5	$7.48997714 \times 10^{-1}$	$-8.036448641 \times 10^{-2}$
a6	$-8.73207040 \times 10^{-1}$	$3.7442365767 \times 10^{-2}$
a7	$1.70609505 \times 10^{-2}$	$-9.2470084512 \times 10^{-4}$
a8	$-1.46355822 \times 10^{-2}$	$5.5047107589 \times 10^{-4}$
a9	$5.79768283 \times 10^{-2}$	$-1.9998708625 \times 10^{-4}$
a10	$-8.41246372 \times 10^{-4}$	$3.4803640287 \times 10^{-5}$
a11	$4.95186474 \times 10^{-3}$	$-2.1485094017 \times 10^{-5}$
a12	$-9.16248538 \times 10^{-3}$	$7.2030001937 \times 10^{-6}$
a13	-1.00358152×10^{-1}	$1.5645721849 \times 10^{-1}$
a14	$-1.82674744 \times 10^{-3}$	$2.6481727363 \times 10^{-3}$
γ	$1.05999998 \times 10^{-2}$	$1.5099999648 \times 10^{-2}$
T _c (K)	647.258	3600
P _c (bar)	221.198	850
V _c (cc/mol)	55.948	295

Table 6
Comparison of the EOS (Eq. 14) of this study with experimental NaCl melt density (g/cm³) by van Artsdalen and Yaffe (1955) and Kirshenbaum et al. (1962).

T (K)	ρ (g/cm ³)		_
	Experiment	EOS(This study)	$\Delta \rho \%$
Data by van Artsdalen and Yaffe (195	5)		
1076.2	1.556	1.5615	-0.35
1083.5	1.5467	1.5516	-0.32
1092.8	1.5457	1.5492	-0.23
1099.1	1.5425	1.5446	-0.14
1102.4	1.5401	1.5422	-0.14
1103.1	1.5397	1.5427	-0.19
1113.7	1.5362	1.5334	0.18
1113.7	1.5361	1.5344	0.11
1118.2	1.5317	1.5311	0.04
1132.3	1.5242	1.5211	0.20
1139.7	1.52	1.5161	0.26
1140.3	1.5198	1.5157	0.27
1144.0	1.5184	1.5134	0.33
1162.3	1.5086	1.5012	0.49
1163.4	1.5074	1.5005	0.46
1163.5	1.5073	1.5005	0.45
1190.0	1.4928	1.4839	0.60
1191.3	1.4921	1.4831	0.60
1195.6	1.4909	1.4805	0.70
1213.0	1.4812	1.4703	0.74
1213.9	1.4798	1.4698	0.68
1213.9	1.4793	1.4690	0.70
1215.3	1.4743	1.4626	0.79
1226.7	1.4661	1.4552	0.74
1240.7	1.4653	1.4551	0.70
1259.3	1.4566	1.4455	0.76
1268.9	1.4494	1.4407	0.60
1278.0	1.4468	1.4363	0.73
1287.2	1.4403	1.4320	0.58
1300.6	1.4322	1.4260	0.43
1189.7	1.4928	1.4839	0.60
1191.3	1.4921	1.4831	0.60
Data by Kirshenbaum et al. (1962)			
1149	1.516	1.5099	0.40
1162	1.503	1.5014	0.11
1202	1.486	1.4767	0.63
1208	1.483	1.4732	0.66
1404	1.388	1.3886	-0.04
1459	1.367	1.3749	-0.58
1502	1.347	1.3669	-1.48
1590	1.305	1.3573	-4.01
1552	1.323	1.3604	-2.83
1573	1.312	1.3585	-3.54
$\Delta \rho\% = 100 \times (\rho_{\it exp} - \rho_{\it calc})/\rho_{\it exp}$			

3.2. EOS of liquid H2O

As previously discussed, the MD molar volumes of H₂O deviate from experimental volumes by less than 1.5 %, which is comparable to individual experimental datasets. However, compared to the average of multiple datasets, the MD results are less accurate. We cannot expect the MD results to be more accurate than the average of many datasets. It is not surprising that well-established models, such as the H₂O model by Wagner and Pruß (2002), are more accurate than a single dataset. However, it only covers the pressure range up to 10 kbar, and extends to 20 kbar with a little less accuracy. What we need is an EOS that is highly accurate up to 30-50 kbar. We once developed an EOS for pure water by fitting MD-simulated data (Zhang and Duan, 2005). It is almost as accurate as the model by Wagner and Pruß (2002) from 1 kbar to 10 kbar and should be reliable up to 100 kbar. The ZD EOS has been used by Sverjensky et al. (2014) in expanding the applicability of the widely used model SUPCRT from 5 kbar to 60 kbar. By adding the newly simulated data from this study to the fitting database of ZD, we did not achieve a significantly better EOS than the original ZD EOS. Since the ZD EOS has already been widely used in various fluid-rock interactions, we decided to maintain consistency and keep the ZD EOS as the endmember EOS for H₂O in this study.

3.3. Mixing rule: EOS of the NaCl-H₂O system

The EOS of the NaCl- H_2O system is composed of the end-member EOS plus a mixing rule. Listed in Table 7 is the mixing rule taken from Duan et al. (1992b). The EOS of the mixture becomes

$$Z = \frac{PV}{RT} = 1 + \frac{BV_c}{V} + \frac{CV_c^2}{V^2} + \frac{DV_c^4}{V^4} + \frac{EV_c^5}{V^5} + \left(\frac{FV_c^2}{V^2} + \frac{GV_c^4}{V^4}\right) \exp\left(-\frac{\gamma V_c^2}{V^2}\right)$$
(16)

where V is molar volume in cm³/mole, P stands for pressure in bar, T for temperature in K, and all other parameters are listed in Table 7. The mixing parameters, k_{ij} , k_{ijk} , k_{ijklm} , and k_{ijklmn} are evaluated from the MD simulated data (Table 3) and the experimental data of Bodnar (1985) up to 6 kbar. The resulting values are in general agreement with other datasets, with deviations less than 1 %. It should be noted that this dataset was not included in the parametrization of the models proposed by Driesner (2007) or Mao et al. (2015).

In the pressure range below 5 kbar, we compared the *PVTx* properties of the EOS of this study with those calculated from well-established models (Anderko and Pitzer, 1993; Mao et al. 2015), as displayed in Table 8. It demonstrates that the EOS of this study is almost as accurate as the other well-established models.

In the high-pressure range from 5 kbar to 30 kbar, the accuracy of the EOS is critical for reliable predictions because both experimental data and theoretical modelling are scarce. As shown in Fig. 3, the EOS of this study can accurately reproduce the acoustic volumetric data at P-T conditions ranging from 5 to 45 kbar and below 673 K.

In conclusion, the EOS developed in this study should exhibit experimental accuracy with uncertainties less than 1.5 %, although additional experimental data are required for further validation in the extremely high *P-T* range. It is important to note that we do not intend to replace existing models with this new model in the pressure range below 5 kbar, as they may possess similar accuracy.

4. Discussion: Geochemical applications of the EOS

As stated above, many critical physicochemical properties can be derived from an EOS. These properties can be instrumental in investigating fluid-rock interactions, examining dehydration and decarbonation reactions within subduction slabs, and studying other fluid-involving processes, where the properties derived from the EOS can serve as intermediaries to enhance the modeling of other variables of geological interest. The following are several such geochemical and geophysical examples that highlight the importance of the EOS.

4.1. H_2O activities derived from the EOS of the NaCl-H2O system for studying fluid-rock interactions, mineral solubility, and dehydration in the crust and upper mantle

Saline fluids are prevalent in various geological settings within subduction zones (e.g., Weiss et al., 2015; Klyukin et al., 2020). Highly saline fluids have been identified across a range of geological environments (e.g., Pasteris et al., 1995; Samson et al., 1995; Fu et al., 2001). Numerous instances of fluid-rock interactions, mineral dehydration reactions, and mineral solubilities can be found in the literature, typically investigated through phase or chemical equilibrium thermodynamic calculations. Generally, the activities of H2O must be derived from thermodynamic models such as EOS proposed by Wagner and Pruß (2002). However, in most cases, salts represented by NaCl are present in geological fluids and may significantly influence H2O activities. As previously mentioned, only a limited number of models exist to calculate volumetric properties or liquid-vapor phase equilibria up to pressures of 5-6 kbar; few can compute activities, and none extend beyond high pressures exceeding 10 kbar. With the EOS developed in this study, it is now feasible to calculate the activity of H2O in saline mixtures at pressures up to 30 kbar and potentially even up to 50 kbar. It has been observed that the impact of NaCl on H2O activity can be substantial.

From the EOS of this study, the total fugacity coefficient can be

Table 7
Mixing rule of Eq. (16).

```
BV_c = \sum \sum_i x_i x_j x_k i_j B_{ij} V_{cij} k_{ij} = 1 (\text{if } i = j) k_{ij} = 0.000106T^2 - 0.128576T + 39.001174 (\text{if } i \neq j \text{ and } T \leq 673 \text{K}) k_{ij} = 0.48 (\text{if } i \neq j \text{ and } T > 673 \text{K}) B_{ij} = ((B_i^{1/3} + B_j^{1/3})/2)^3 V_{cij} = ((V_{ci}^{1/3} + V_{cj}^{1/3})/2)^3 V_{cijk} = ((V_{ci}^{1/3} + V_{ck}^{1/3})/3)^3 V_{cijk} = ((V_{ci}^{1/3} + V_{ci}^{1/3})/3)^3 V_{cijk} = ((V_{ci}^{
```

Table 8
Comparison of the EOS of this study with those of models below 5 kbar from Anderko and Pitzer (1993) and Mao et al. (2015).

T(K)	P (kbar)	$V (cm^3/m$	ole)		T (K)	P (kbar)	$V (cm^3/m$	V (cm ³ /mole)		
		AP	Mao et al.	This study	-		AP	Mao et al	This study	
$m_{\text{NaCl}} = 1$.423 wt% NaCl =	$7.68 x_{\text{NaCl}} = 0.0$	025		$m_{NaCl} = 1$	3.9 wt% NaCl = 4	$4.8 x_{\text{NaCl}} = 0.2$	0		
573	1	21.4	21.4	22	573	3		20.65	21.6	
573	2	20.3	20.2	20.7	573	5		20.3	21	
573	3	19.7	19.37	19.8	673	3	21.8	21.7	22.3	
573	5	18.8	18.3	18.5	673	5	21	21.2	21.6	
673	2	22	22.2	22.01	873	3	24.4	24	23.7	
673	3	21.1	20.9	20.9	873	5	23	23.1	22.6	
673	4	20.4	20.1	20.01	1073	3	27.7	27.1	26.5	
673	5	19.9	19.4	19.34	1073	5	25.3	25.2	24.5	
873	3	25.3	25.2	25.6	1173	3	29.7	28.7	27.9	
873	5	22.4	22.1	22.4	1173	5	26.41	26.37	25.9	
1073	3	31.6	31	31.8	1273	3		30.5	30.3	
1073	5	25.8	25.4	25.9	1273	5		27.6	27.1	
1173	3	35.4	34.27	35.4	1573	5		31.3	33	
1173	5	27.8	27.25	27.8	$m_{NaCl} = 3$	7 wt% NaCl = 68.	$8 x_{\text{NaCl}} = 0.40$			
1273	3		37.64	39.3	573	3		23.2	25	
1273	5		29.2	29.9	573	5		23.3	24.6	
$m_{NaCl}=3$	$wt\%\ NaCl = 14.6$	$x_{\text{NaCl}} = 0.051$			673	3		24.01	25.6	
573	2	20.5	20.2	20.8	673	5		24.05	25.4	
573	3	19.9	19.45	19.9	873	3	25.7	25.9	26.5	
573	4	19.5	19	19.3	873	5	24.9	25.7	25.8	
573	5	19.1	18.51	18.75	1073	3	27.9	28	27.8	
673	2	22.1	21.9	21.6	1073	5	26.5	27.4	26.6	
673	3	21.1	20.9	20.7	1173	3	29.1	29.1	28.9	
673	4	20.4	20.1	20.01	1173	5	27.3	28.3	27.5	
673	5	19.9	19.6	19.4	1273	3		30.3	30.3	
873	3	25.3	24.6	25	1273	5		29.2	28.6	
873	5	22.4	22.1	22.3	1573	5				
1073	3	30.6	29.7	30.5	$m_{NaCl} = 8$	2.9 wt% NaCl = 8	$3.3 x_{\text{NaCl}} = 0.60$	0		
1073	5	25.8	25.1	25.5	573	3		26.1	27.7	
1173	3	34.2	32.6	34.1	573	5		26.21	27.4	
1173	5	27.4	26.8	27.4	673	3		26.87	29.56	
1273	3		35.6	37.9	673	5		26.99	29.17	
1273	5		28.5	29.5	873	3		28.59	30.28	
1573	5			36.3	873	5		28.58	29.59	
$m_{NaCl}=6$.17 wt% NaCl = 2	$x_{NaCl} = 0.10$	0		973	3	29.1	29.5	30.91	
573	1	21.4	21.2	21.6	973	5	28.2	29.4	30	
573	3	20.3	19.7	20.3	1073	3	30	30.41	31.7	
573	5	19.6	19.3	19.3	1073	5	28.9	30.21	30.6	
673	3	21.2	20.96	20.8	1173	3	30.9	31.36	32.75	
673	5	20.2	20.01	19.8	1173	5	29.6	31.02	31.45	
873	3	24.6	24.1	24	1273	3		32.2	33.87	
873	5	226	22.3	22.32	1273	5		31.84	32.33	
1073	3	29.2	28.1	28.1	1573	5		34.29	34.86	
1073	5	25.4	24.9	24.7						
1173	3	32.1	30.5	31.2						
1173	5	26.9	26.3	26.4						
1273	3		32.9	34.7						
1273	5		27.8	28.4						

derived from the EOS:

$$ln\Phi = \int_{P_{ref}}^{P} \frac{v}{RT} dP = ln\Phi_{P} - ln\Phi_{ref}$$
 (17)

where $ln\Phi_P$ or $ln\Phi_{ref}$ are calculated as

$$ln\Phi_{\textit{PorP}_{ref}} = z - 1 - ln(z) + \frac{BV_c}{V} + \frac{CV_c^2}{2V^2} + \frac{DV_c^4}{4V^4} + \frac{EV_c^5}{5V^5}$$

$$-\frac{FV_c^2}{2\gamma V_c^2}\left[1-\exp\!\left(-\frac{\gamma V_c^2}{V^2}\right)\right] - \frac{\left(\gamma V_c^2 G V_c^4 + G V_c^4 V^2\right)}{2(\gamma V_c^2)^2 V^2} \exp\!\left(-\frac{\gamma V_c^2}{V^2}\right)_{\textit{PorP}_{\textit{pof}}}$$

Since the EOS only covers the pressure range above 1 kbar, so $P_{ref}=1kbar$. To maintain consistency with the EOS of the end-member $\rm H_2O$, we have adopted a reference state of 2 kbar.

$$ln\phi_{i} = ln\Phi - x_{j\neq i} \left(\frac{\partial ln\Phi}{\partial x_{j}}\right)_{T,P,x_{i\neq j}}$$
(18)

Where z = PV/RT, $ln\Phi$ is the natural logarithm of the fugacity coeffi-

cient of the whole system and $ln\phi_i$ is that of the partial fugacity coefficient of the components: H_2O and NaCl in the mixture. $x_{j\neq i}$ is the mole fraction of species j, which is different from species i. The parameters such as BV_c and CV_c^2 are listed in Table 7. The activity of H_2O is calculated by

$$a_{H_2O} = \frac{\phi_{H_2O} x_{H_2O}}{\phi_{H_2O}^0} \tag{19}$$

where $\phi_{H_2O}^0$ denotes pure water fugacity coefficient, and ϕ_{H_2O} refers to fugacity coefficient of water in NaCl-H₂O mixtures at the same temperature, pressure and NaCl concentrations. Eqs. (17–19) can be used to calculate water activities which should find many applications in mineral solubility, fluid-rock interaction, dehydration, and any phase or chemical reactions associated with NaCl-bearing aqueous systems, as long as the species in the aqueous liquid are identified.

A comparison with the experimental measurements of H_2O activity reported by Aranovich and Newton (1996) and the values calculated with Eqs. (17–19) as shown by Fig. 4, demonstrated a general

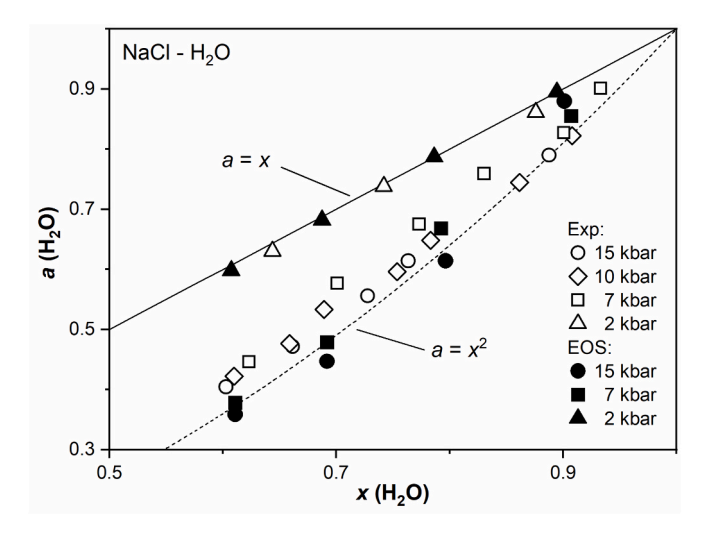


Fig. 4. Comparison the calculated ${\rm H_2O}$ activity under different pressures with experimental measurements under different pressures.

consistency: in the low pressure range, $a_{H_2O} \approx x_{H_2O}$, but under high P conditions, $a_{H_2O} \approx x_{H_2O}^2$.

4.2. A revised conductivity model to analyze the salinity and filling rate of geological fluids in subduction zones and the Earth's crust

The study of the electrical conductivity of NaCl-H₂O solutions serves as a valuable tool for predicting the conductivity of deep saline fluids, which has significant implications for the analysis of salt concentration and fluid composition within continental crust, island arcs, and subduction zones. The development of conductivity models for NaCl-H2O plays a crucial role in clarifying the distribution of deep Earth fluids. High-conductivity zones have frequently been identified in the Earth's crust, as well as in arc and subduction regions, using magneto-telluric and seismic data (e.g., Soyer and Unsworth, 2006; Le Pape et al., 2012; Meqbel et al., 2014). Typically, these anomalous electrical conductivities can be related to the presence of NaCl-H₂O fluids, as aqueous solutions generally have significantly higher conductivities than solid rocks (Sakuma and Ichiki, 2016). Even a tiny amount of NaCl-H2O fluid can lead to a dramatic increase in the electrical conductivity of an area, which is influenced by the conductivity of the fluid and its fraction or filling rate (e.g., Guo et al., 2015; Sun et al., 2020). By integrating magneto-telluric data with conductivity models of NaCl-H2O solutions, we can investigate the salinity and fraction of NaCl-H2O fluids in regions of high conductivity or the filling rate of interstitial cavities, facilitating research on plate tectonics, mineral distribution, and earthquake prediction.

The density of NaCl- $\rm H_2O$ solutions is a critical parameter affecting their conductivity (Quist and Marshall, 1968; Bannard, 1975). However, due to the lack of a density calculation model for NaCl- $\rm H_2O$ solutions under conditions of high temperature and pressure, current models used to calculate the conductivity of NaCl- $\rm H_2O$ solutions often rely on the density of pure water in their calculations (e.g., Sinmyo and Keppler, 2017; Guo and Keppler, 2019) or propose empirical or semi-empirical formulas that neglect density terms altogether (Sakuma and Ichiki, 2016; Watanabe et al., 2021). These computational formulas tend to be quite complex and may be constrained in their scope of application.

With the density of NaCl- H_2O mixtures derived from the EOS developed in this study, we are now able to model the conductivity of NaCl- H_2O solutions with a much more efficient and accurate formula:

$$\log \sigma = A + B \log T + C \log c + D\rho + E\rho^2 + F\rho^3$$
(20)

where σ is the conductivity (S/m), T is the temperature (K), c is wt% of

NaCl, ρ is the density of NaCl-H₂O solution (g/cm³), and A-F are parameters (A = 6.620, B = 1.325, C = 0.792, D = -28.626, E = 27.225, and F = -8.149) evaluated from the data of Sinmyo and Keppler (2017) and Guo and Keppler (2019), covering 473–1173 K in temperature, 0.2–5 GPa in pressure, and 0.058–5.5 in NaCl mass fraction. Comparing Eq. (20) with all experimental data except those in the low temperature (<100 °C) and high pressure (> 4 GPa) ranges, all 187 sets of data are well reproduced as shown in Fig. 5. For comparison, the previous commonly used models are also shown in the same figure.

For further comparison, the absolute error values of each data point were calculated, and the mean absolute error of the conductivity in logarithmic form is shown in Table 9, which also includes the mean absolute errors of the previous models of Sinmyo and Keppler (2017) and Guo and Keppler (2019). The values in parentheses are the extrapolated values of the respective models and are not within the applicable range set by the models. Table 10 shows the number of parameters and the range of different models, including some models that do not use the density term. As seen from Table 9 and Table 10, the model of this study is applicable within the overall range of 0.2–5 GPa, and the mean absolute error in the ranges of 0.2–1 GPa and 1–5 GPa is more accurate with fewer parameters compared to the previous models.

Overall, based on the new EOS of this study, we are able to obtain a revised conductivity model with fewer parameters, higher accuracy, and a broader range of *P-T* range. As with previous models, this model (Eq. (17)) is expected to find wide applications in the studies of salinity and filling rate of fluids in subduction zones and Earth's crust.

4.3. Fluid inclusion studies

Ultra-high density (or high pressure) fluids have been found in diamond inclusions (e.g., Tomlinson et al., 2006; Weiss et al., 2015), eclogites (e.g., Fu et al., 2001), and other rocks formed in deep Earth. Isochores calculated from EOSes or empirical models have long been used to trace the formation temperatures or pressures of minerals or rocks (Roedder and Bodnar, 1980; Bodnar, 1985). These models, including those of Zhang and Frantz (1987), Anderko and Pitzer (1993), Driesner (2007), Steele-MacInnis et al. (2012), are all limited below 6 kbar. Extending these models to higher pressures often relies on linear extrapolation, the reliability of which remains uncertain. The only work covering up to 12 kbar is that of Li et al. (2024). By extending from the approximately 6 kbar limit of most thermodynamic models to 30 kbar, the EOS of this study greatly extends P-T coverage for such fluid studies.

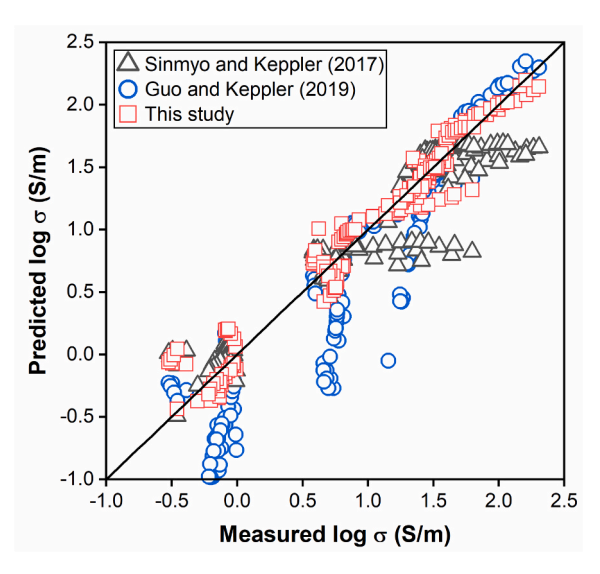


Fig. 5. Comparison of our new conductivity model (Eq. (20) with experimental data, indicating our new model is more accurate than previous models, but spans larger *P-T* range with fewer parameters.

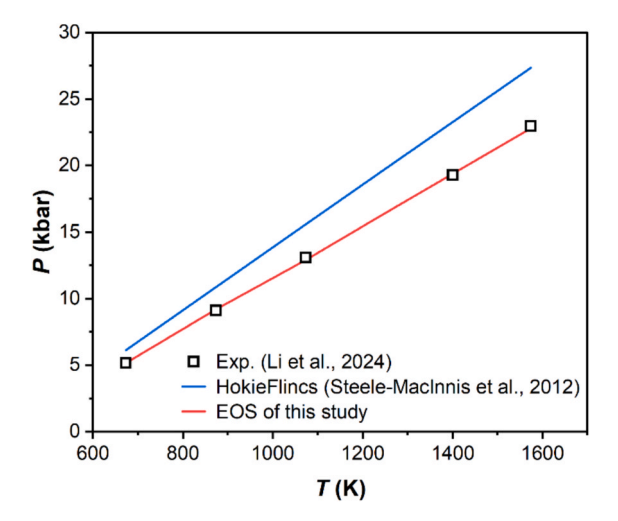


Fig. 6. The isochores calculated from the EOS are highly consistent with the new HDAC data up to high pressures, potentially the new EOS may provide a better model for the study of fluid inclusions.

Table 9The absolute errors of the conductivity model (Eq. (17) with previous models.

Models	Mean absolute error (%)				
	0.2-1GPa	1-5GPa	0.2-5GPa		
Sinmyo and Keppler (2017) Guo and Keppler (2019)	9.6 (51.2)	(22.9) 16.7	(16.6) (33.1)		
This study	7.8	14.7	11.4		

Table 10Comparison of conductivity model (Eq. (17) of this study with previous models.

Models	T(K)	P(GPa)	NaCl wt%	# of para.
Sakuma and Ichiki (2016)	673-2000	0.2-2	0.6-9.6	27
Sinmyo and Keppler (2017)	373-873	0.2-1	0.058 - 5.5	8
Guo and Keppler (2019)	373-1173	1–5	0.058 - 5.5	8
Watanabe et al. (2021)	20-525	0.025 - 0.2	0.059-24.6	10
This study	473-1173	0.2 - 5	0.058 - 5.5	6

This new EOS, which is validated by the well-established models of Anderko and Pitzer (1993), Driesner (2007), and Mao et al. (2015) below 6 kbar. It has also been verified using experimental data of Li et al. (2024) up to 12 kbar (Fig. 6), Mantegazzi et al. (2013) up to 45 kbar (Table 11), and the MD simulated data as discussed in Section 2. We believe that this new EOS should serve as a new criterion for assessing the efficacy of these models with respect to linear extension. Here, we choose the high salinity fluid inclusions in coesite-bearing eclogites (Dabieshan, China) as an example (Fu et al., 2001). The average ice melting temperature is -20 °C (T_m) and the vapor-to-liquid homogenization temperature is about 140 °C (T_h). Based on the T_m and T_h , isochores calculated from the model of Steele-MacInnis et al. (2012) and from experimental data of Li et al. (2024) are drawn in Fig. 6, which shows the P-T path calculated from the EOS of this study is highly consistent with the experimental data.

5. Concluding remarks and Perspectives

5.1. on the predictability of MD together with EOS

Due to the widespread presence of NaCl- H_2O fluids in various geological settings and the significance of their thermodynamic properties in interpreting physicochemical mechanisms in geological processes, over forty PVTx or density measurement datasets have been

Table 11Comparison of the EOS of this study and previous models with the experimental results of Mantegazzi et al. (2013).

T(K)	P (kbar)	Fowler and Sherman	Fowler and Sherman (ab initio)	Sakuma and IChiki	This study	Exp. (g/ cm ³)
$m_{ ext{NaCl}} = 1$		$\rho(\Delta\rho\%)$	$\rho(\Delta\rho\%)$	$\rho(\Delta\rho\%)$	$\rho(\Delta\rho\%)$	ρ
573	5			1.05 (-1.94)	1.02 (0.97 %)	1.03
573	11			1.18 (-0.85)	1.15 (-1.7	1.17
573	21			1.33 (-2.31)	%) 1.29 (0.77)	1.3
573	31			1.44 (-3.60)	1.38 (0.72)	1.39
673	5		1.098 (13.00)	1.00 (-3.13)	0.97 (0.00)	0.97
673	11		1.189 (-5.22)	1.13 (0.00)	1.11 (1.77)	1.13
673	21		1.260 (-2.69)	1.26 (0.79)	1.25 (1.57)	1.27
673	31		(2.03)	1.35 (1.46)	1.35 (1.46)	1.37
673	41		1.454(-0.3)	1.43 (0.69)	1.43 (0.69)	1.44
673	45		1.476(-0.4)	1.45 (1.36)	1.45 (1.36)	1.47
$m_{\text{NaCl}} = 3$				(====)	(=14-4)	
573	5			1.12 (-2.75)	1.07 (1.83)	1.09
573	11			1.25 (-1.63)	1.21 (1.63)	1.23
573	21			1.4 (-2.19)	1.36 (0.73)	1.37
573	31			1.52 (-4.83)	1.43 (1.38)	1.45
673	5	1.01(1.94	1.151 (-11.6)	1.06 (-2.91)	1.04 (-0.97)	1.03
673	11	1.15(4.17)	1.250 (-4.17)	1.2(0.00)	1.18 (1.67)	1.20
673	17	1.24 (-0.81)	1.323 (-7.56)	1.29 (-4.88)	1.26 (-2.43)	1.23
673	21			1.33 (0.75)	1.31 (-2.24)	1.34
673	29	1.36 (-0.74)		1.41 (-4.44)	1.39 (2.96)	1.35
673	31	,,		1.42 (0.70)	1.41 (1.40)	1.43
673	45	1.48(3.9)	1.538(0.13)	1.52 (1.30)	1.52 (1.30)	1.54
$\Delta \rho \% = 1$	$100 imes (ho_{exp}$	$(\rho_{calc})/\rho_{exp}$				

published by more than 30 laboratories, and more than ten empirical or semi-empirical models have been developed for this binary system over the past half-century. However, as illustrated in Fig. 7, the measurements or models generally fall within the range below 5–6 kbar (Area I in Fig. 7). Only two sets of experimental *PVTx* data have been found in the high-pressure, low-temperature region (Area II in Fig. 7). There is almost no data available in the extensive high *P-T* range, as shown in Area III of Fig. 7.

We have demonstrated that the EOS is competitive with the best models in P-T range I (as shown in Table 10). In P-T range II, the EOS also shows high agreement with experimental data up to 45 kbar (as indicated in Table 11). Although we lack experimental data to validate the reliability of the EOS in P-T range III, the MD simulated data should, to a large extent, serve a similar role as experimental data due to their comparable accuracy. Additionally, we did not treat P-T range III differently from ranges I and II, where the EOS was proven to be as accurate as experimental data. In summary, the EOS of the NaCl-H₂O system developed in this study should exhibit accuracy close to

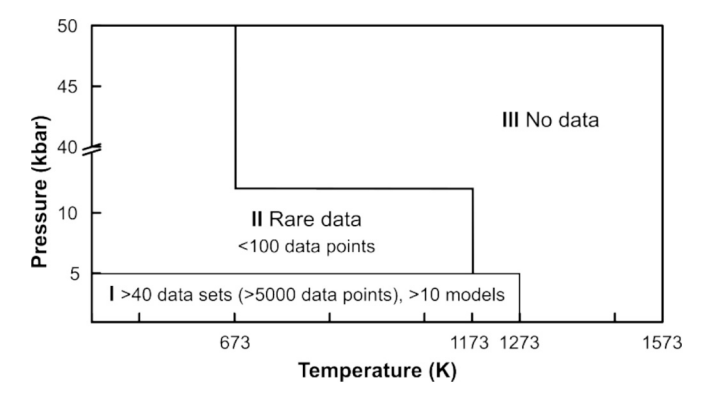


Fig. 7. P-T coverage of experimental data of the NaCl-H₂O system. The EOS of this study covers the whole P-T range (including I, II, and III) above 573 K and 1 kbar.

experimental data across the range of 573 to 1573 K, 1 kbar to 30 kbar (possibly up to 50 kbar), and 0 to 1 $x_{\rm NaCl}$ though more experimental data are useful for further validations.

We conclude from above that MD simulations can yield thermodynamic properties in a large PVTx range, which in turn can be used to build an EOS that can interpolate experimental data and extrapolate far beyond the data range. The research process, beginning with the examination of fundamental water properties (ice moduli, the second virial coefficient, and spectra) and progressing to the evaluation of potential developments (e.g., RWK2 developed by Watts et al.), culminates in the utilization of molecular dynamics computer simulations to derive PVTx properties (Table 3). This comprehensive approach has been employed to develop the EOS of the system NaCl-H₂O across a wide range of temperatures and pressures, thereby underscoring the efficacy and predictability of the MD + EOS methodology.

5.2. Perspectives

As discussed in Section 4, the EOS of this study has the potential to be utilized in a multitude of geochemical and geophysical applications, such as predicting mineral solubilities and fluid-rock interactions, development of electric conductivity models for the crust and upper mantle or subduction fluids, and fluid-inclusion studies up to high P-T conditions.

With the flexible RWK2 potential and the ionic potential programmed, it is feasible to investigate other properties, such as bond-vibrations or Raman spectroscopy of $\rm H_2O$ molecules, transport properties (diffusion and viscosity), liquid structure (radial distribution function and cation—anion association properties, such as ion-pairing), as well as how these properties vary with temperature, pressure, and ionic strength. Additionally, it is worth examining whether these properties can be studied with the same degree of accuracy as that of the PVTx properties. The intention is to pursue further investigation and seek resolutions to these questions in the near future.

CRediT authorship contribution statement

Zhenhao Duan: Writing – review & editing, Writing – original draft, Validation, Supervision, Software, Resources, Project administration, Methodology, Investigation, Funding acquisition, Formal analysis, Data curation, Conceptualization. Nanfei Cheng: Writing – review & editing, Visualization, Validation, Funding acquisition. Zhigang Zhang: Writing – review & editing, Validation, Software. I-Ming Chou: Writing – review & editing, Funding acquisition. Haoran Sun: Writing – review & editing, Visualization, Validation.

Declaration of competing interest

The authors declare that they have no known competing financial interests or personal relationships that could have appeared to influence the work reported in this paper.

Acknowledgments

We are grateful to Dr. Gleb Pokrovski, Dr. David M. Sherman, and two anonymous reviewers for their valuable insights and constructive suggestions, which have significantly enhanced the quality of this manuscript. Dr. Jiangzhi Chen is thanked for the assistance with solving technical issues of supercomputing. This research was supported by the Project of the Institute of Deep-sea Science and Engineering, Chinese Academy of Sciences (grant number IDSSE-SJBS-202402) and the National Natural Science Foundation of China (grant numbers 42130109 and 42102056).

Appendix A. Supplementary material

Supplementary material to this article can be found online at htt ps://doi.org/10.1016/j.gca.2025.10.022.

References

Abdulagatov, I.M., Dvoryanchikov, V.I., Mursalov, B.A., Kamalov, A.N., 1998.
Measurements of heat capacities at constant volume for aqueous salt solutions H2O-NaCl, H2O-KCl and H2O-NaOH near the critical point of pure water. Fluid Phase Equilib. 143 (1998), 213–239.

Adams, L.H., 1931. Equilibrium in binary systems under pressure. I. an experimental and thermodynamic investigation of the system, NaCl- $\rm H_2O$, at 25° . J. Am. Chem. Soc. 53, 3769–3813.

Allen, M.P., Tildesley, D.J., 1987. Computer simulation of liquids, first Ed. Oxford University Press, New York.

Aranovich, L.Y., Newton, R.C., 1996. H₂O activity in concentrated NaCl solutions at high pressures and temperatures measured by the brucite-periclase equilibrium. Contrib. to Mineral. Petrol. 125, 200–212.

Arcis, H., Bachet, M., Dickinson, S., Duncanson, I., Eaker, R.W., Jarvis, J., Johnson, K., Lee, C.A., Lord, F., Marks, C., Tremaine, P.R., 2024. Revised parameters for the IAPWS formulation for the ionization constant of water over a wide range of temperatures and densities, including near-critical conditions. J. Phys. Chem. Ref. Data 53, 023103.

Anderko, A., Pitzer, K.S., 1993. Equation-of-state representation of phase equilibria and volumetric properties of the system NaCl-H₂O above 573 K. Geochim. Cosmochim. Acta 57, 1657–1680.

Bakker, R.J., 2003. Package FLUIDS 1. Computer programs for analysis of fluid inclusion data and for modelling bulk fluid properties. Chem. Geol. 525, 400–413.

Bannard, J.E., 1975. Effect of density on the electrical conductance of aqueous sodium chloride solutions. J. Appl. Electrochem. 5, 43–53.

Belonoshko, A., Saxena, S.K., 1991a. A molecular dynamics study of the pressure-volume-temperature properties of super-critical fluids: I. H2O. Geochim. Cosmochim. Acta 55, 381–387.

Belonoshko, A., Saxena, S.K., 1991b. A molecular dynamics study of the pressure-volume-temperature properties of supercritical fluids: II. CO₂, CH₄, CO, O₂, and H₂. Geochim. Cosmochim. Acta 55, 3191–3208.

Bischoff, J.L., Pitzer, K.S., 1989. Liquid-vapor relations for the system NaCl-H₂O: summary of the P-T- x surface from 300° to 500°C. Am. J. Sci. 289, 217–248.

Bischoff, J.L., 1991. Densities of liquids and vapors in boiling NaCl-H₂O Solutions: a PVTX summary from 300° to 500°C. Am. J. Sci. 291, 309–338.

Bockris, J.O., Richards, N.E., 1957. The compressibilities, free volumes and equation of state for molten electrolytes: some alkali halides and nitrates. *Proc. R. Soc. A Math.* Phys. Eng. Sci. 241, 44–66.

Bodnar, R.J., 1985. Pressure-volume-temperature-composition (PVTX) properties of the system H20-NaCl at elevated temperatures and pressures. Pennsylvania State University. Ph.D. dissertation.

Bodnar, R.J., 1995. Fluid-inclusion evidence for a magmatic source for metals in porphyry copper deposits. In: Thompson, J.F. (Ed.), Magmas, Fluids and Ore Deposits, Volume 23. Mineralogical Association of Canada Short Course, np. 139–152.

Cheng, N., Jenkins, D.M., Huang, F., 2019. Dehydration of glaucophane in the system Na₂O–MgO–Al₂O₃–SiO₂–H₂O and the effects of NaCl-, CO₂- and silicate-bearing aqueous fluids. J. Petrol. 60, 2369–2386.

Chou, I.-M., 1987. Phase relations in the system NaCl-KCl-H₂O. III: Solubilities of halite in vapor-saturated liquids above 445 °C and redetermination of phase equilibrium properties in the system NaCl-H₂O to 1000 °C and 1500 bars. Geochim. Cosmochim. Acta 51, 1965–1975.

Coker, D.F., Watts, R.O., 1987. Structure and vibrational spectroscopy of the water dimer using quantum simulation. J. Phys. Chem. 91, 2513–2518.

- Ditler, E., Luber, S., 2022. Vibrational spectroscopy by means of first-principles molecular dynamics simulations. Wiley Interdiscip. Rev.: Comput. Mol. Sci. V5, 1605
- Driesner, T., 2007. The system H_2O -NaCl. Part II: Correlations for molar volume, enthalpy, and isobaric heat capacity from 0 to 1000°C, 1 to 5000bar, and 0 to 1 $X_{\rm NaCl}$. Geochim. Cosmochim. Acta 71, 4902–4919.
- Driesner, T., Heinrich, C.A., 2007. The system $\rm H_2O-NaCl$. Part I: Correlation formulae for phase relations in temperature–pressure–composition space from 0 to $1000\,^{\circ}$ C, 0 to 5000 bar, and 0 to $1\, X_{\rm NaCl}$. Geochim. Cosmochim. Acta 71, 4880–4901.
- Duan, Z., Møller, N., Weare, J.H., 1992a. An equation of state for the CH₄-CO₂-H₂O system: I. Pure systems from 0 to 1000°C and 0 to 8000 bar. Geochim. Cosmochim. Acta 56, 2605–2617.
- Duan, Z., Møller, N., Weare, J.H., 1992b. Molecular dynamics simulation of PVT properties of geological fluids and a general equation of state of nonpolar and weakly polar gases up to 2000 K and 20,000 bar. Geochim. Cosmochim. Acta 56, 3839–3845.
- Duan, Z., Møller, N., Wears, J.H., 1995. Molecular dynamics simulation of water properties using RWK2 potential: from clusters to bulk water. Geochim. Cosmochim. Acta 59, 3273–3283.
- Duan, Z., Møller, N., Weare, J.H., 1996. A general equation of state for supercritical fluid mixtures and molecular dynamics simulation of mixture *PVTX* properties. Geochim. Cosmochim. Acta 60, 1209–1216.
- Duan, Z., Møller, N., Weare, J.H., 2003. Equations of state for the NaCl-H₂O-CH₄ system and the NaCl-H₂O-CO₂-CH₄ system: phase equilibria and volumetric properties above 573 K. Geochim. Cosmochim. Acta 67, 671–680.
- Duan, Z., Møller, N., Weare, J.H., 2004. Gibbs Ensemble Simulations of Vapor/Liquid Equilibrium using the Flexible RWK2 Water potential. J. Phy. Chem. B 108, 20303–20309.
- Fowler, S.J., Sherman, D.M., 2020. The nature of NaCl-H2O deep fluids from abinitio molecular dynamics at 0.5-4.5 GPa, 20-800 and 1-14m NaCl. Geochimi. Cosmochimi. Acta. 277, 243–264.
- Fu, B., Touret, J.L.R., Zheng, Y.F., 2001. Fluid inclusions in coesite-bearing ecologites and jadeeite quartzite at Shuanghe, Dabie shan (China). J. Metamorphic Geol. 19, 531–547
- Guo, H., Keppler, H., 2019. Electrical conductivity of NaCl-bearing aqueous fluids to 900 and 5 GPa. J. Geophys. Res. Solid Earth 124, 1397–1411.
- Guo, X., Yoshino, T., Shimojuku, A., 2015. Electrical conductivity of albite-(quartz)—water and albite-water-NaCl systems and its implication to the high conductivity anomalies in the continental crust. Earth Planet. Sc. Lett. 412, 1–9.
- Haar, L., Gallagher, J.S., Kell, G.S., 1984. NBS/NRC Steam Tables. Taylor & Francis, London. p. 320.
- Hamann, S.D., 1963. The ionization of water at high pressures. J. Phys. Chem. 67, 2233–2235.
- Helgeson, H.C., Delany, J.M., Nesbitt, H.W., Bird, D.K., 1978. Summary and critique of the thermodynamic properties of rock-forming minerals. Am. J. Sci. 278A, 569–592.
- Huang, F., Sverjensky, D.A., 2019. Extended Deep Earth Water Model for predicting major element mantle metasomatism. Geochim. Cosmochim. Acta 254, 192–230.
- Janz, G.J., 1980. Molten salts data as reference standards for density, surface tension, viscosity and electrical conductance: $\rm KNO_3$ and NaCl. J. Phys. Chem. Ref. Data 9, 791–830.
- Johnson, J.W., Oelkers, E.H., Helgeson, H.C., 1992. SUPCRT92: a software package for calculating the standard molal thermodynamic properties of minerals, gases, aqueous species, and reactions from 1 to 5000 bar and 0 to 1000°C. Comput. Geosci. 18, 899–947.
- Kaplan, I.G., 2006. Intermolecular Interactions: Physical Picture. Wiley, Computational Methods and Model Potentials.
- Keevil, N.B., 1942. Vapor pressures of aqueous solutions at high temperatures. J. Am. Chem. Soc. 64, 841–850.
- Kirshenbaum, A.D., Cahill, J.A., McGonigal, P.J., Grosse, A.V., 1962. The density of liquid NaCl and KCl and an estimate of their critical constants together with those of the other alkali halides. J. Inorg. Nucl. Chem. 24, 1287–1296.
- Klyukin, Y.I., Harold, E.L., Steele-MacInnis, 2020. A comprehensive numerical model for the thermodynamic and transport properties of H2O-NaCl fluids. Chem. Geol. 557, 1–5.
- Lan, T., An, Q., 2021. Discovering Catalytic Reaction Networks using Deep Reinforcement Learning from First-Principles. J. Ame Chem Society v143, 16804–16812.
- Le Pape, F., Jones, A.G., Vozar, J., Wenbo, W., 2012. Penetration of crustal melt beyond the Kunlun Fault into northern Tibet. Nat. Geosci. 5, 330–335.
- Li, J., Chou, I.-M., Wang, X., 2024. In-situ determination of NaCl-H₂O isochores up to 900 and 1.2 GPa in a hydrothermal diamond-anvil cell. Geochem. Perspect. Lett. 31, 32–37.
- Li, M., Duan, Z., Zhang, Z., Zhang, C., Weare, J., 2008. The structure, dynamics and solvation mechanisms of ions in water from long time molecular dynamics simulations: a case study of CaCl₂ (aq) aqueous solutions. Mol. Phys. 106, 2685–2697.
- Manning, C.E., Aranovich, L.Y., 2014. Brines at high pressure and temperature: Thermodynamic, petrologic and geochemical effect. Precambr. Res. 253, 6–16.
- Mantegazzi, D., Sanchez-Valle, C., Driesner, T., 2013. Thermodynamic properties of aqueous NaCl solutions to 1073 K and 4.5 GPa, and implications for dehydration reactions in subducting slabs. Geochim. Cosmochim. Acta 121, 263–290.
- Mao, S., Duan, Z., 2008. The P,V,t,x properties of binary aqueous chloride solutions up to T=573K and 100MPa. J. Chem. Thermodyn. 40, 1046–1063.
- Mao, S., Duan, Z., Hu, J., Zhang, D., 2010. A model for single-phase *PVTx* properties of CO₂-CH₄-C₂H₆-N₂-H₂O-NaCl fluid mixtures from 273 to 1273 K and from 1 to 5000 bar. Chem. Geol. 275, 148–160.

- Mao, S., Hu, J., Zhang, Y., Lü, M., 2015. A predictive model for the PVTx properties of CO₂-H₂O-NaCl fluid mixture up to high temperature and high pressure. Appl. Geochem. 54, 54–64.
- Mao, W., Zhong, H., Ulrich, T., 2023. Evolutionary paths for the formation of different types of fluid inclusions in the H₂O-NaCl system. Ore Geol. Rev. 159, 105561.
- Meqbel, N.M., Egbert, G.D., Wannamaker, P.E., Kelbert, A., Schultz, A., 2014. Deep electrical resistivity structure of the northwestern US derived from 3-D inversion of USArray magnetotelluric data. Earth Planet. Sc. Lett. 402, 290–304.
- Mei, Y., Liu, W., Chopping, R., 2019. Equation-of-state and electrical conductivity of NaCl-bearing fluids in the deep Earth: insights from molecular simulations. ASEG Ext. Abstr. 2019, 1–4.
- Moore, E.W., Ross, J.W., 1965. NaCl and CaCl₂ activity coefficients in mixed aqueous solutions. J. Appl. Physiol. 20, 1332–1336.
- Ni, P., Ding, J., Rao, B., 2006. In situ cryogenic Raman spectroscopic studies on the synthetic fluid inclusions in the systems H₂O and NaCl-H₂O. Chinese Sci. Bull. 51, 108–114.
- Newton, R.C., Manning, C.E., 2000. Quartz solubility in H₂O-NaCl and H₂O-CO₂ solutions at deep crust-upper mantle pressures and temperatures: 2-15 kbar and 500-900°C. Geochim. Cosmochim. Acta 64, 2993–3005.
- Pan, D., Spanu, L., Harrison, B., Sverjensky, D.A., Galli, G., 2013. Dielectric properties of water under extreme conditions and transport of carbonates in the deep Earth. Proc. Natl. Acad. Sci. 110, 6646–6650.
- Pan, D., Galli, G., 2020. A first principles method to determine speciation of carbonates in supercritical water. Nature Comm. 11, 421.
- Parkhurst, D.L., Appelo, C.A.J., 1999. User's guide to PHREEQC (Version 2): a computer program for speciation, batch-reaction, one-dimensional transport, and inverse geochemical calculations. U.S, Geological Survey, Denver CO.
- Pasteris, J.D., Harris, T.N., Sassari, D.C., 1995. Interactions of mixed volatile-brine fluids in rocks of the southwestern footwall of the Duluth complex, Minnesota – evidence from aqueous fluid inclusions. Am. J. Sci. 295, 125–172.
- Pitzer, K.S., Li, Y., 1983. Thermodynamics of aqueous sodium chloride to 823 K and 1 kilobar (100 MPa). Proc. Natl. Acad. Sci. 80, 7689–7693.
- Pitzer, K.S., Pabalan, R.T., 1986. Thermodynamics of NaCl in steam. Geochim. Cosmochim. Acta 50, 1445–1454.
- Pitzer, K.S., Peiper, J.C., Busey, R.H., 1984. Thermodynamic properties of aqueous sodium chloride solutions. J. Phys. Chem. Ref. Data 13, 1–102.
- Qiu, Z., Fan, H., Tomkins, A.G., Etschmann, B., Liu, X., Xing, Y., Hu, Y., 2021. Insights into salty metamorphic fluid evolution from scapolite in the Trans-North China Orogen: Implication for ore genesis. Geochim. Cosmochim. Acta 293, 256–276.
- Quist, A.S., Marshall, W.L., 1968. Electrical conductance of aqueous sodium chloride solutions from 0 to 800. degree. and at pressures to 4000 bars. J. Phys. Chem. 72, 684–703.
- Reimers, J.R., Watts, R.O., Klein, M.L., 1982. Intermolecular potential functions and the properties of water. Chem. Phys. 64, 95–114.
- Robie R. A. and Hemingway B. S., 1995 Thermodynamic properties of minerals and related substances at 298.15 K and 1 bar (10^5 pascals) pressure and at higher temperatures. U.S. Geological Survey Bulletin 2131, Denver, CO.
- Roedder, E., Bodnar, R.J., 1980. Geologic pressure determinations from fluid inclusion studies. Ann. Rev. Earth Plan. Sci. 8, 263–301.
- Sakuma, H., Ichiki, M., 2016. Density and isothermal compressibility of supercritical H2O-NaCl fluid: molecular dynamics study from 673 to 2000 K, 0.2 to 2 GPa, and 0 to 22 wt% NaCl concentrations. Geodluids 16, 89–102.
- Samson, I.M., Liu, W., Williams-Jones, A.E., 1995. The nature of orthomagmatic fluids in the Oka carbonatite, Quebec, Canada: evidence from fluid inclusions. Geochim. Cosmochim. Acta 59, 1963–1977.
- Schulze, M., Driesner, T., Jahn, S., 2024. Assessing the validity and limits of linear density models for predicting dissociation—association equilibria in supercritical water. Geochim. Cosmochim, Acta. In press.
- Schulze, M., Jahn, S., 2024. Speciation and dynamic properties of hydrous $MgCO_3$ melt studied by ab-initio molecular dynamics. Geochim. Cosmochim. Acta 368, 147–155.
- Sherman, Collings, 2002. Ion association in concentrated NaCl brines from ambient to supercritical conditions: results from classical molecular dynamics simulations. Geochem. Trans. 3, 102–107.
- Shi, X., Zhang, L., Hu, J., Mao, S., 2024. A model for the solubilities of corundum in aqueous NaCl and/or SiO_2 solutions and its implication for the mobility of aluminum at depth. Chem. Geol. 663, 122257.
- Shock, E.L., Oelkers, E.H., Johnson, J.W., Sverjensky, D.A., Helgeson, H.C., 1992. Calculation of the thermodynamic properties of aqueous species at high pressures and temperatures. Effective electrostatic radii, dissociation constants and standard partial molal properties to 1000 °C and 5 kbar. J. Chem. Soc. Faraday Trans. 88, 803–826.
- Shock, E.L., Sassani, D.C., Willis, M., Sverjensky, D.A., 1997. Inorganic species in geologic fluids: Correlations among standard molal thermodynamic properties of aqueous ions and hydroxide complexes. Geochim. Cosmochim. Acta 61, 907–950.
- Shu, Q., Chang, Z., Mavrogenes, J., 2021. Fluid compositions reveal fluid nature, metal deposition mechanisms, and mineralization potential: an example at the Haobugao Zn-Pb skarn, China. Geology 49, 473–477.
- Smith, D.E., Dang, L.X., 1994. Computer simulations of NaCl association in polarizable water. J. Chem. Phys. 100, 3757–3766.
- Soyer, W., Unsworth, M., 2006. Deep electrical structure of the northern Cascadia (British Columbia, Canada) subduction zone: Implications for the distribution of fluids. Geology 34, 53–56.
- Steele-MacInnis, M., Lecumberri-Sanchez, P., Bodnar, R.J., 2012. HokieFlincs H2O-NaCl: a microsoft excel spreadsheet for interpreting microscopic data from fluid inclusions based on the *PVTX* properties of H2O-NaCl. Comput. Geosci. 49, 334–337.

- Sinmyo, R., Keppler, H., 2017. Electrical conductivity of NaCl-bearing aqueous fluids to $600\,^{\circ}\text{C}$ and 1 GPa. Contrib. to Mineral. Petrol. 172, 4.
- Sverjensky, D.A., Harrison, B., Azzolini, D., 2014. Water in the deep Earth: the dielectric constant and the solubilities of quartz and corundum to 60 kb and 1200 $^{\circ}$ C. Geochim. Cosmochim. Acta 129, 125–145.
- Sverjensky, D.A., Huang, F., 2015. Diamond formation due to a pH drop during fluid-rock interactions. Nat. Commun. 6, 8702.
- Sverjensky, D.A., Shock, E.L., Helgeson, H.C., 1997. Prediction of the thermodynamic properties of aqueous metal complexes to 1000°C and 5 kb. Geochim. Cosmochim. Acta 61, 1359–1412.
- Sun, W., Dai, L., Li, H., Hu, H., Jiang, J., Wang, M., 2020. Electrical conductivity of clinopyroxene-NaCl- $\rm H_2O$ system at high temperatures and pressures: Implications for high-conductivity anomalies in the deep crust and subduction zone. J. Geophys. Res. Solid Earth 125, e2019JB019093.
- Tödheide, K., 1980. The influence of density and temperature on the properties of pure molten salts. Angew. Chemie Int. Ed. English 19, 606–619.
- Tomlinson, E.L., Jones, A.P., Harris, J.W., 2006. Co-existing fluid and silicate inclusions in mantle diamond. Earth Planet. Sci. Lett. 250, 581–595.
- Van Artsdalen, E.R., Yaffe, I.S., 1955. Electrical conductance and density of molten salt systems: KCl-LiCl, KCl-NaCl and KCl-KI. J. Phys. Chem. 59, 118–127.
- Vega, A., Abascal, J.L.F., 2011. Simulating water with rigid non-polarizable models: a general perspective Phys. Chem. Chem. Phys. 13, 19663–19688.

- Wagner, W., Pruß, A., 2002. The IAPWS formulation 1995 for the thermodynamic properties of ordinary water substance for general and scientific use. J. Phys. Chem. Ref. Data 31, 387–535.
- Watanabe, N., Yamaya, Y., Kitamura, K., Mogi, T., 2021. Viscosity-dependent empirical formula for electrical conductivity of H₂O-NaCl fluids at elevated temperatures and high salinity. Fluid Phase Equilibr. 549, 113187.
- Weiss, Y., McNeill, J., Pearson, D.G., Nowell, G.M., Ottley, C.J., 2015. Highly saline fluids from a subducting slab as the source for fluid-rich diamonds. Nature 524, 339–342.
- Yardley, B.W.D., Graham, J.T., 2002. The origins of salinity in metamorphic fluids. Geofluids 2, 249–256.
- Zheng, Y.-F., 2009. Fluid regime in continental subduction zones: petrological insights from ultrahigh-pressure metamorphic rocks. J. Geol. Soc. London 166, 763–782.
- Zhang, Z., Duan, Z., 2005. Prediction of the *PVT* properties of water over wide range of temperatures and pressures from molecular dynamics simulation. Phys. Earth Planet. In. 149, 335–354.
- Zhang, Y.-G., Frantz, J.D., 1987. Determination of the homogenization temperatures and densities of supercritical fluids in the system NaCl-KCl-CaCl2-H2O using synthetic fluid inclusions. Chem. Geol. 64, 335–350.
- Zimmer, K., Zhang, Y., Lu, P., Chen, Y., Zhang, G., Dalkilic, M., Zhu, C., 2016. SUPCRTBL: a revised and extended thermodynamic dataset and software package of SUPCRT92. Comput. Geosci. 90, 97–111.